NACA

RESEARCH MEMORANDUM

AERODYNAMIC CHARACTERISTICS AT TRANSONIC AND SUPERSONIC SPEEDS OF A ROCKET-PROPELLED AIRPLANE CONFIGURATION HAVING A DIAMOND-PLAN-FORM WING OF ASPECT RATIO 3.08 AND A LOW, SWEPT HORIZONTAL TAIL

By Alan B. Kehlet

Langley Aeronautical Laboratory
Langley Field, Va.

NATIONAL ADVISORY COMMITTEE
FOR AERONAUTICS

WASHINGTON
September 10, 1954

[redacted]

NATIONAL ADVISORY COMMITTEE FOR AERONAUTICS

RESEARCH MEMORANDUM

AERODYNAMIC CHARACTERISTICS AT TRANSONIC AND SUPERSONIC SPEEDS OF A ROCKET-PROPELLED AIRPLANE CONFIGURATION HAVING A DIAMOND-PLAN-FORM WING OF ASPECT RATIO 3.08 AND A LOW, SWEPT HORIZONTAL TAIL

By Alan B. Kehlet

SUMMARY

A flight investigation over a Mach number range from 0.95 to 1.79 has been conducted to determine the aerodynamic characteristics of a rocket-propelled model of an airplane configuration having a diamond-plan-form wing of aspect ratio 3.08 with NACA 65A003 airfoil sections in the free-stream direction and a low, swept horizontal tail. The lift-curve slopes were nonlinear with lift coefficient over the lift range covered and decreased with increasing lift coefficient. The static-longitudinal-stability parameters were nonlinear with lift coefficient and the stability increased with lift coefficient. Near a Mach number of 0.95 at the low-lift tail setting and negative lift coefficients, the model exhibited an unstable break in the pitching-moment curve and pitched down.

The model exhibited greater longitudinal damping when at the higher lift tail setting than at the low-lift tail setting.

Comparison of wing-plan-form effects was made between the model of the present investigation and a previously reported delta-wing model. The greatest plan-form effect was on the static stability.

INTRODUCTION

As part of a general research program investigating longitudinal stability of wings having various plan forms (ref. 1) and thickness ratios, a rocket-propelled model of an airplane configuration having a diamond-plan-form wing of aspect ratio 3.08 has been flight tested over a Mach number range of 0.95 to 1.79 at Reynolds numbers of 5×10^6 to

[redacted]

[redacted]

15×10^6. The basic fuselage-empennage configuration had swept horizontal and vertical tails with the all-movable horizontal tail mounted in a low position. During the flight, the horizontal tail was deflected in a square-wave program between stops of approximately 0.1° and -3.4°.

The model in the present investigation was almost identical in mass and geometric characteristics to the delta-wing model of reference 1. Because of the similarity of the two models, comparison figures are presented which show the effect of wing plan form on the aerodynamic characteristics of the configuration.

The model was flown at the Langley Pilotless Aircraft Research Station at Wallops Island, Va.

SYMBOLS

C_N	normal-force coefficient, $\frac{a_n}{g}\frac{W/S}{q}$
C_C	chord-force coefficient, $-\frac{a_l}{g}\frac{W/S}{q}$
C_L	lift coefficient, $C_N \cos \alpha - C_C \sin \alpha$
C_D	drag coefficient, $C_C \cos \alpha + C_N \sin \alpha$
C_m	pitching-moment coefficient about center of gravity
C_Y	side-force coefficient, $\frac{a_t}{g}\frac{W/S}{q}$
a_n	normal acceleration determined from accelerometer, ft/sec^2
a_l	longitudinal acceleration determined from accelerometer, ft/sec^2
a_t	transverse acceleration determined from accelerometer, ft/sec^2
g	acceleration due to gravity, ft/sec^2
q	dynamic pressure, $0.70pM^2$
p	free-stream static pressure, lb/sq ft
M	Mach number

[redacted]

$(L/D)_{max}$ maximum lift-drag ratio

L lift, lb

D drag, lb

A aspect ratio

S wing area (including area enclosed by fuselage), sq ft

$\bar{c}$ wing mean aerodynamic chord, ft

W weight, lb

$T_{1/2}$ time to damp to one-half amplitude, sec

V velocity, ft/sec

α angle of attack, deg

δ control panel deflection (measured in plane parallel to fuselage plane of symmetry), deg

θ angle of pitch, radians

β angle of sideslip, deg

$C_{m_q} = \frac{dC_m}{d\left(\frac{q\bar{c}}{2V}\right)}$, per radian

$C_{m_{\dot{\alpha}}} = \frac{dC_m}{d\left(\frac{\dot{\alpha}\bar{c}}{2V}\right)}$, per radian

$C_{n_\beta}{}^*$ effective rate of change of yawing-moment coefficient with sideslip angle (derived as in ref. 6), per deg

$\frac{dC_D}{dC_L{}^2}$ effect of lift on drag

C_{m_α} rate of change of pitching-moment coefficient about center of gravity with angle of attack (determined from period method), per deg

Subscripts:

$\dot{\alpha}$ $\frac{1}{57.3}\frac{d\alpha}{dt}$

q $\frac{d\theta}{dt}$ when used in the damping term

The symbols α and δ, used as subscripts indicate the derivative of the quantity with respect to the subscript; for example, $C_{L_\alpha} = \frac{dC_L}{d\alpha}$.

MODEL

A three-view drawing of the model is shown in figure 1. Photographs of the model are shown in figure 2.

The empennage and fuselage are described in references 1 and 2, respectively.

The steel diamond-plan-form wing of aspect ratio 3.08 had a leading-edge sweep of 33° with the 50-percent-chord line unswept and NACA 65A003 airfoil sections in the streamwise direction. The diamond-plan-form wing and the delta wing of reference 1 were designed, and positioned on the models, so that both wings had the same span, aspect ratio, and mean-aerodynamic-chord station.

Each panel of the horizontal tail was deflected in an approximate square-wave program by a separate servo control fed by a common pressure system and regulated by an electric motor-driven selector valve. For the present investigation, the stop positions were approximately 0.1° and −3.4° measured in a plane parallel to the fuselage plane of symmetry.

The model weighed 118.25 pounds and had moments of inertia in pitch and yaw of 8.14 and 8.37 slug-ft^2, respectively. The center of gravity was located at the same station as 0.25 of the wing mean aerodynamic chord.

INSTRUMENTATION

The model was equipped with an NACA telemetering system which transmitted continuous measurements of normal acceleration at the center of gravity, normal acceleration at a reference nose station, angle of attack, longitudinal acceleration, transverse acceleration, control position,

total pressure (high range), total pressure (low range), and reference static pressure.

Flight-path information was obtained from tracking radar and atmospheric conditions at altitude from a radiosonde released immediately after the flight.

TESTS AND DATA REDUCTION

Preflight Tests

Prior to flight testing and with the instruments installed, the model was suspended by shock cords and vibrated by an electromagnetic shaker. The following model natural frequencies were determined:

	First bending, cps	Second bending, cps
Vertical tail	62.5	
Horizontal tail	100	
Wing	150	350

Flight Tests

The model was launched at an angle of approximately 60° from the horizontal by means of a mobile launcher as shown in figure 2(b). Two 6-inch-diameter solid-fuel ABL Deacon rocket motors boosted the model to maximum velocity. At booster burnout, the model separated from the booster and was thereafter in free coasting flight.

Data Reduction

The response of the model to deflections of an all-movable horizontal tail in an approximate square-wave program was analyzed by the method of reference 3. The indicated angles of attack were corrected to angles of attack at the model center of gravity by the method of reference 4. The two-accelerometer method for obtaining instantaneous total pitching-moment coefficients was used as described in reference 2. All measurements used were taken during the decelerating portion of the flight.

[redacted]

Accuracy

The absolute accuracy of the measured quantities is impossible to establish because the instrument calibrations cannot be checked during or after the flight. Most of the probable instrumentation errors occur as errors in absolute magnitude. Incremental values or slopes should, in general, be more accurate than absolute values. An indication of the systematic instrument errors possible is given by the following table, based on an accuracy of ±1 percent of the full instrument range:

M	C_N	C_C
1.7	±0.0047	±0.0012
1.4	±.0081	±.0020
1.0	±.0200	±.0050

The CW Doppler radar unit is believed to be accurate to better than 1 percent for nonmaneuvering models. The Mach number at peak velocity should, therefore, be accurate to 1 percent or better. Mach number subsequent to peak velocity was determined from the telemetric data of the high- and low-range pressure cells and is believed accurate to about 2 percent at M = 1.00.

Further errors in the aerodynamic coefficients may arise from possible dynamic-pressure inaccuracies which are approximately twice as great as errors in Mach number.

An indication of random errors encountered may be noted from the scatter of data points shown in the figures. Errors in angle of attack and horizontal-tail deflection are independent of dynamic pressure and are not likely to vary with Mach number. The horizontal-tail deflections are estimated to be accurate within ±0.10° and angle of attack within ±0.20°.

RESULTS AND DISCUSSION

Dynamic pressure and Reynolds number obtained during the flight are shown in figures 3 and 4, respectively. The Reynolds number range covered during the flight was from about 5×10^6 to 15×10^6.

A time history of some of the quantities measured in the present investigation is shown in figure 5. Throughout the flight, the model exhibited lateral oscillations when pulsed in pitch. Near $M = 0.95$ at negative lift coefficients with the 0.1° tail setting, the model pitched down and oscillated violently in the lateral plane. The resulting motions were such that no further useful longitudinal-stability data could be obtained. The angle-of-attack data after the model pitched down have been dashed to distinguish them from the lift and side-force coefficients.

The variation of the trim lift coefficient and trim angle of attack at the two tail settings as functions of Mach number is shown in figure 6. At transonic speeds and with increasing Mach number, the model exhibited a smooth nose-up change in trim of approximately 3° at the 0.1° tail setting and a nose-down change in trim of approximately 4° at the -3.4° tail setting.

In order to distinguish the two trim conditions, the data are presented as a function of tail setting even though the primary factor is the difference in the trim lift coefficients. Presentation of data as a function of tail setting is done because it was not possible throughout the flight to cover two constant lift coefficients with two tail settings. Hereinafter, the deflection of 0.1° shall be referred to as the low-lift tail setting and the deflection of -3.4° as the higher lift tail setting.

Lift

The variation of the lift coefficient with angle of attack at the two tail settings over the Mach number range is shown in figure 7. Although some hysteresis is present in some of the oscillations, slopes through data exhibiting hysteresis and faired slopes are the same. The lift-curve slopes at trim lift coefficients, represented by the faired lines in figure 7, are presented as functions of Mach number in figure 8 for both tail settings.

It is evident from figure 8 that the lift coefficient does not vary linearly with angle of attack, with the lower lift tail setting having the greater value of lift-curve slope.

The lift-curve slopes of a diamond-plan-form wing of aspect ratio 4 (ref. 5), taken at model trim lift coefficients, indicates that the nonlinearity is due, in a large part, to the wing alone, with a decrease in lift-curve slope with increasing angle of attack. It is believed that the downwash effect on the low tail should lessen as angle of attack is increased, giving rise to an increasingly higher lift-curve slope as angle of attack is increased (assuming a linear lift-curve slope of the wing and tail alone); however, in the present investigation, it is

believed that the decreasing lift-curve slope of the wing with angle of attack more than offsets any lift increase due to a decrease in downwash over the tail.

Drag

The variation of drag coefficient with lift coefficient corresponding to the lift ranges of figure 7 is shown in figure 9. The maximum lift-drag ratios and the lift coefficients at which $(L/D)_{max}$ occurs are shown as a function of Mach number in figure 10. The maximum lift-drag ratio decreased from about 8 at $M = 0.95$ to about $4\frac{1}{2}$ at $M = 1.54$; lift coefficients corresponding to these values are about 0.29 and 0.33, respectively.

The minimum drag coefficient obtained from figure 9 is presented as a function of Mach number in figure 11. The minimum drag coefficient increased from about 0.02 near $M = 0.95$ to 0.038 near $M = 1.08$ and decreased slowly with increasing Mach number. The values of the lift coefficient at minimum drag coefficient were essentially zero.

The effect of lift on drag as a function of Mach number is presented in figure 12. The model exhibited little or no leading-edge suction.

Longitudinal Static Stability

The variation of the measured periods of the longitudinal oscillations at the two tail settings is shown as a function of Mach number in figure 13. Periods could not be measured at Mach numbers less than 0.99 because of pitch-down of the model at negative lift. The variation of C_{m_α} as determined from these periods is shown as a function of Mach number in figure 14. As with the lift-curve slopes (fig. 8), the C_{m_α} data exhibited nonlinearity with lift coefficient. Throughout the Mach number range covered, the model at the higher lift tail setting exhibited the greater static stability with an essentially constant value of C_{m_α} of about -0.0175. Values of C_{m_α} at the low-lift tail setting increased with increasing Mach number from about -0.006 at $M = 1.04$ to about -0.018 at $M = 1.78$.

The variation of the static-stability parameter C_{m_α} is reflected in the aerodynamic-center location (as determined from the lift-curve slopes and C_{m_α} derived from the period data) at both tail settings (fig. 15). All data exhibited a rearward movement of the aerodynamic center with increasing Mach number over the lift and Mach number ranges covered. It should be noted that the model exhibited a low value of static stability near $M = 1.03$ at the low-lift condition. About

M = 0.95, at negative lift with the low-lift tail setting, the model pitched down.

The variation of the total pitching-moment coefficient (as determined by the two-accelerometer method) with lift coefficient at the two tail settings is shown in figure 16. Although some scatter is present, generally the data agree with the slopes of the period method above M = 1.005 at the higher lift tail setting and above M = 1.173 at the low-lift tail setting.

At the higher lift tail setting below M = 1.25, the slope of the pitching-moment curve shows a tendency to increase with increasing lift coefficient over the lift range covered (fig. 16(a)). The steeper slope would indicate an increase in model static stability. The increase in stability with increasing C_L for a model having a low tail is consistent with the thought of a decreasing downwash effect on the tail with increasing lift coefficient.

Near M = 1.06 at the low-lift tail setting, a decrease in model static stability with increasing negative lift coefficients becomes evident (fig. 16(b)). Near M = 0.95, the Mach number where the model pitched down, an unstable break in the pitching-moment curve occurs at negative lift coefficients greater than -0.45. The pitch-down at negative lift coefficients of a model having a low tail is analogous to the pitch-up at positive lift coefficients of a model having a slightly high tail.

A measure of the horizontal-tail effectiveness in producing moment and ability to produce lift, as obtained by the method described in reference 1, is shown in figure 17. Values could be obtained only above M = 1.05. Both parameters exhibit the same general shape as the lift-curve slopes (fig. 8).

Damping in Pitch

The time to damp to one-half amplitude (determined as described in ref. 1) and the pitch damping-moment factor as functions of Mach number are presened in figure 18. Values of $T_{1/2}$ at both tail settings decreased with increasing Mach number, with the higher lift tail setting exhibiting the greater total damping. No data were obtained near M = 1.05 for the model at the low-lift tail setting due to the long period at this Mach number. The variations of $T_{1/2}$ are reflected in the pitch damping-moment factor $C_{m_q} + C_{m_{\dot{\alpha}}}$ with the data at the higher lift tail setting indicating the greater damping, in agreement with the data of reference 1.

[redacted]

The time history of figure 5 shows some lateral oscillations existing throughout the flight, which introduces the possibility of coupling between longitudinal and lateral oscillations. The effect of coupling is believed to tend to distort the model damping.

Directional Static Stability

As in reference 1, lateral oscillations were also present in this investigation. The variation of the measured periods of these oscillations and the static-directional-stability derivative (derived as in ref. 6) are presented in figures 19 and 20, respectively. Throughout the Mach number range, the periods appear to be unaffected by lift coefficient over the lift range covered.

The static-directional-stability derivative exhibited a decrease of about 50 percent from the peak transonic value to the maximum Mach number. This large decrease is believed to be due in part to the increased effect of flexibility of the vertical tail with increased Mach number. Reference to the table of natural frequencies indicates a rather flexible vertical tail. At the Mach numbers covered, however, the model exhibited stable static directional characteristics.

An estimation of the approximate maximum amplitudes of sideslip angle over the Mach number range covered indicates values of about $\pm 0.6^\circ$ above $M = 1.3$ and increasing to about $\pm 1.0^\circ$ below this Mach number.

Comparison of Wing Plan Forms

The diamond-plan-form-wing model of the present investigation and the delta-wing model of reference 1 were almost identical with the exception of wing plan form. The two wings had the same aspect ratio, taper ratio, and airfoil sections. Because of the basic similarities in both models, comparison figures are presented to show the effect of wing plan form on the aerodynamic characteristics of the configuration. Center-of-gravity locations of the diamond-wing model and the delta-wing model of reference 1 were 0.25 and 0.26 of the wing mean aerodynamic chord, respectively. A plan-form view of the two models superimposed is shown in figure 21.

The variation of the longitudinal trim conditions at each tail setting for the two models is presented in figure 22 as a function of Mach number. The diamond-wing model of the present investigation trimmed at higher C_L at the higher lift tail setting and lower C_L at the low-lift tail setting than the delta-wing model of reference 1 at the same respective tail settings. Although there exists a slight difference in the higher lift tail settings of the two models, the

difference in trim is primarily due to the respective static stability of each model and both models are in the same general lift range.

The variation of the lift-curve slopes of the two models as a function of Mach number is presented in figure 23. Above $M = 1.10$ at the higher lift tail setting, the lift-curve slopes of the two wings are the same. At Mach numbers greater than $M = 1.40$, where the trim lift coefficients of the two models are about the same, values of the lift-curve slope of the diamond-wing model at both tail settings are equal or greater than values from the delta-wing model of reference 1. Throughout the Mach number range, regardless of trim lift coefficient, values of C_{L_α} of the diamond-wing model at the low-lift condition were greater than those of reference 1 at the same tail setting. The difference at low-lift is believed to be due to a higher lift-curve slope of the diamond-wing alone.

The variation of maximum lift-drag ratios and lift coefficients at which maximum lift-drag ratios occur as a function of Mach number for the two models is presented in figure 24. Above $M = 1.10$, wing plan form apparently has little effect on the values of the two parameters. In the Mach number range less than $M = 1.10$, the effect of wing plan form is intensified, with the diamond-wing model exhibiting a lower $(L/D)_{max}$ and higher C_L for $(L/D)_{max}$ than the delta-wing model of reference 1.

The variation of minimum drag coefficient and the effect of lift on drag for both models are shown as a function of Mach number in figures 25 and 26, respectively. Throughout most of the Mach number range, the diamond-wing model exhibits a higher minimum drag coefficient than the delta-wing model. Both wing plan forms exhibit approximately the same values of $\frac{dC_D}{dC_L^2}$ (fig. 26) and in each case exhibit little or no leading-edge suction.

The variation of the horizontal-tail effectiveness in producing moment as a function of Mach number for both models is presented in figure 27. The results are identical over the Mach number range covered by each model.

The variation of aerodynamic center as a function of Mach number for each model is presented in figure 28. Throughout the Mach number range regardless of tail setting, the delta-wing model of reference 1 exhibited the more rearward aerodynamic-center location. The more forward location of the aerodynamic center of the diamond-wing model is believed to be due to the forward location of the center of pressure of the wing alone (ref. 5) and to higher downwash over the horizontal tail.

The variation of the pitch damping-moment factors for each model as a function of Mach number is shown in figure 29. Over the Mach number range covered by each model, the diamond-wing model at the higher lift tail setting exhibited the greater values of $C_{m_q} + C_{m_{\dot{\alpha}}}$. Since both models oscillated in the lateral mode when pulsed in pitch and coupling effects on the damping are probably present, effects of wing plan form on damping in pitch cannot be accurately evaluated.

The variation of the static-directional-stability derivative for each model as a function of Mach number is presented in figure 30. Over the Mach number ranges covered, values of C_{n_β}* of the two models are in good agreement. As would be expected with two models with vertical tails of about equal flexibility, wing plan form has little effect on the directional static stability.

CONCLUSIONS

A flight investigation of the aerodynamic characteristics at transonic and supersonic speeds of a rocket-propelled airplane configuration having a diamond-plan-form wing of aspect ratio 3.08 and a low, swept horizontal tail indicates the following conclusions:

1. Near a Mach number of 0.95 at negative lift with the low-lift tail setting, the model pitched down and oscillated violently in the lateral plane.

2. The lift-curve slopes were nonlinear throughout the Mach number range and decreased with increasing lift coefficient.

3. The maximum lift-drag ratios decreased from about 8 near a Mach number of 0.95 to about $4\frac{1}{2}$ near a Mach number of 1.54 with corresponding lift coefficients of about 0.29 and 0.33, respectively.

4. Over the Mach number range where it could be determined, the model exhibited little or no leading-edge suction.

5. With increasing Mach number, the aerodynamic center moved rearward with greater stability at the higher lifts.

6. The model exhibited greater damping characteristics at the higher lift tail setting than at the low-lift tail setting.

7. The model exhibited stable static directional characteristics over the Mach number and lift ranges covered.

8. The largest effect of wing plan form on two almost identical models, one having a diamond-plan-form wing and the other a delta wing, was a more rearward aerodynamic-center location for the delta-wing model.

Langley Aeronautical Laboratory,
National Advisory Committee for Aeronautics,
Langley Field, Va., July 9, 1954.

REFERENCES

1. Kehlet, Alan B.: Aerodynamic Characteristics at Transonic and Supersonic Speeds of a Rocket-Propelled Airplane Configuration Having a 52.5° Delta Wing and a Low, Swept Horizontal Tail. NACA RM L54A20, 1954.

2. Vitale, A. James: Effects of Wing Elasticity on the Aerodynamic Characteristics of an Airplane Configuration Having 45° Sweptback Wings As Obtained From Free-Flight Rocket-Model Tests at Transonic Speeds. NACA RM L52L30, 1953.

3. Gillis, Clarence L., Peck, Robert F., and Vitale, A. James: Preliminary Results From a Free-Flight Investigation at Transonic and Supersonic Speeds of the Longitudinal Stability and Control Characteristics of an Airplane Configuration With a Thin Straight Wing of Aspect Ratio 3. NACA RM L9K25a, 1950.

4. Mitchell, Jesse L., and Peck, Robert F.: An NACA Vane-Type Angle-of-Attack Indicator for Use at Subsonic and Supersonic Speeds. NACA RM L9F28a, 1949.

5. Few, Albert G., Jr., and Fournier, Paul G.: Effects of Sweep and Thickness on the Static Longitudinal Aerodynamic Characteristics of a Series of Thin, Low-Aspect-Ratio, Highly Tapered Wings at Transonic Speeds - Transonic-Bump Method. NACA RM L54B25, 1954.

6. Purser, Paul E., and Mitchell, Jesse L.: Miscellaneous Directional-Stability Data for Several Airplane-Like Configurations From Rocket-Model Tests at Transonic Speeds. NACA RM L52E06b, 1952.

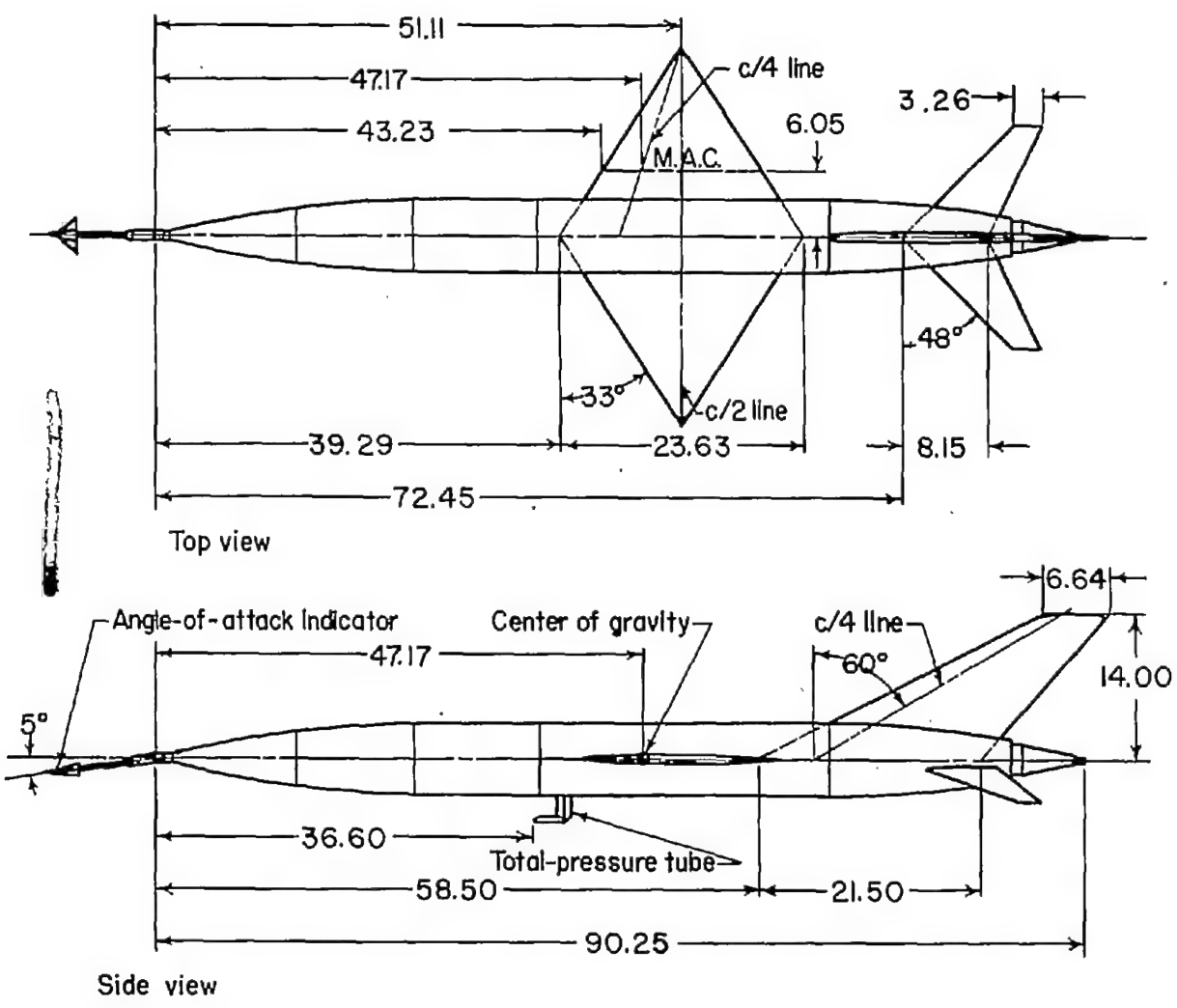

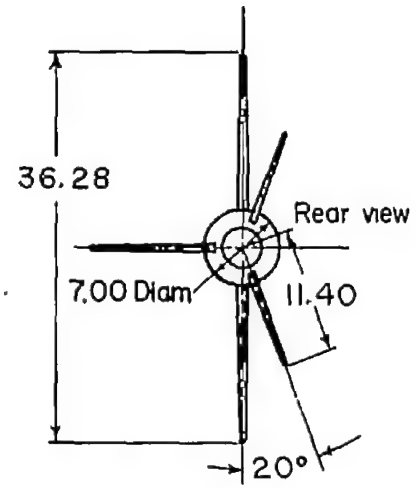

Wing		
Aspect ratio	3.08	
Area (total)	2.982	sq ft
Area (exp)	1.942	sq ft
Dihedral	0.0	deg
M.A.C.	1.314	ft
Airfoil section	NACA 65A 003	
Horizontal tail		
Aspect ratio	4.00	
Area (total)	0.905	sq ft
Dihedral	-2 0.0	deg
M.A.C.	0.504	ft
Airfoil section	NACA 65A 006	
Vertical tail		
Area (total)	1.37	sq ft
Airfoil section	NACA 65A 003	

Figure 1.- General arrangement of model. All dimensions in inches.

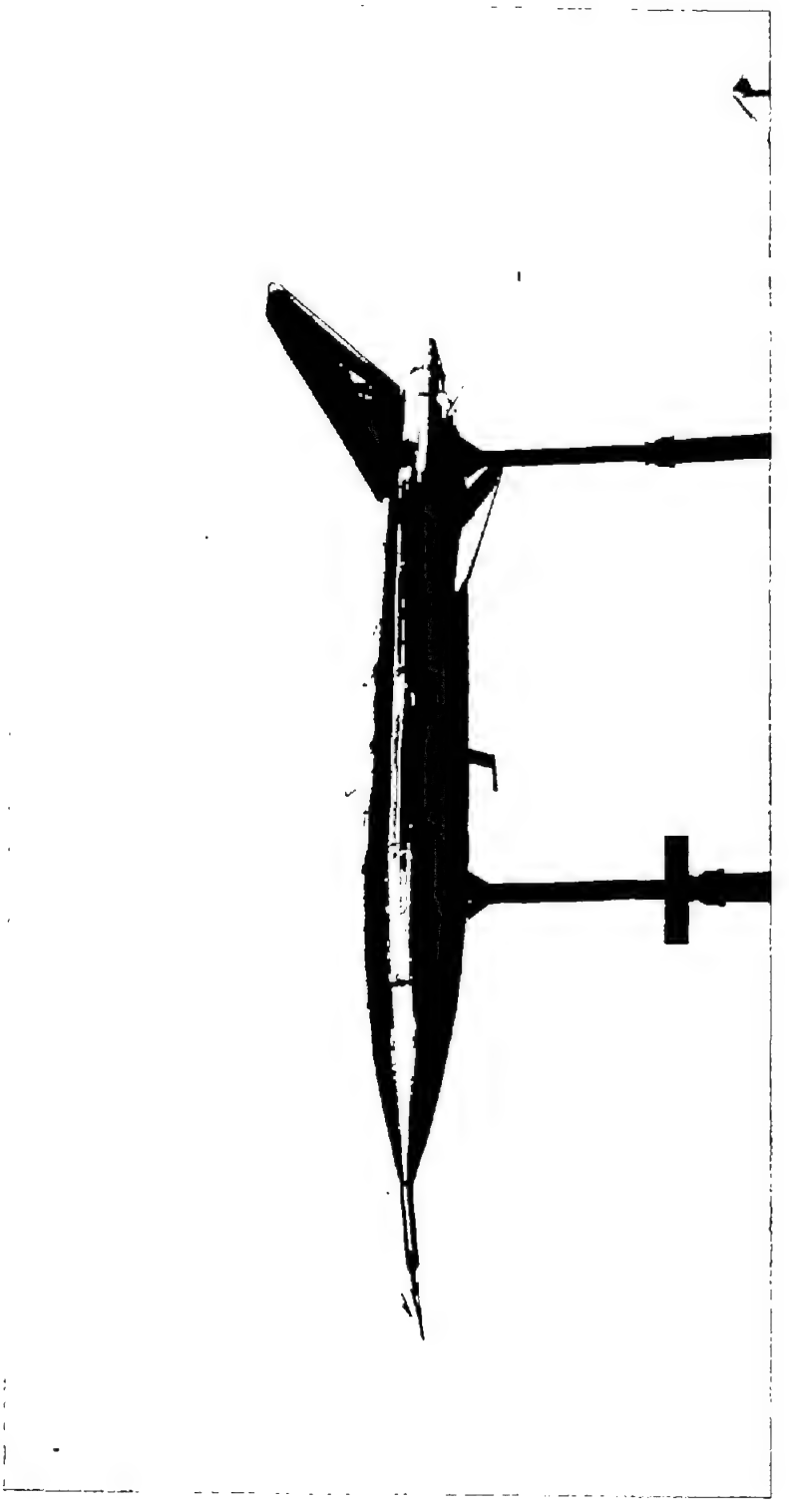

L-80897.1

(a) Three-quarter front view.

Figure 2.- Photographs of model.

[redacted]

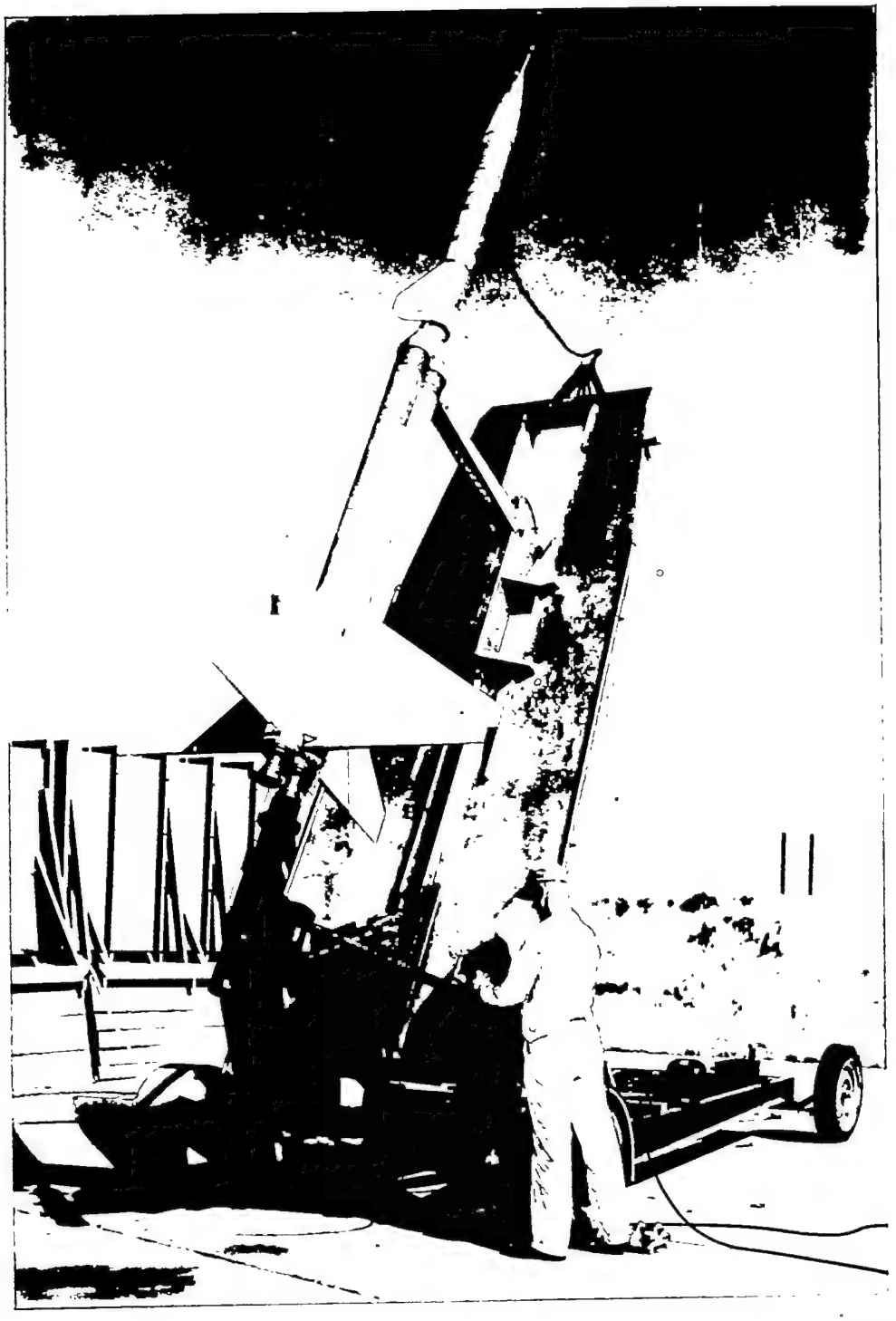

L-81595.1

(b) Model on launcher.

Figure 2.- Concluded.

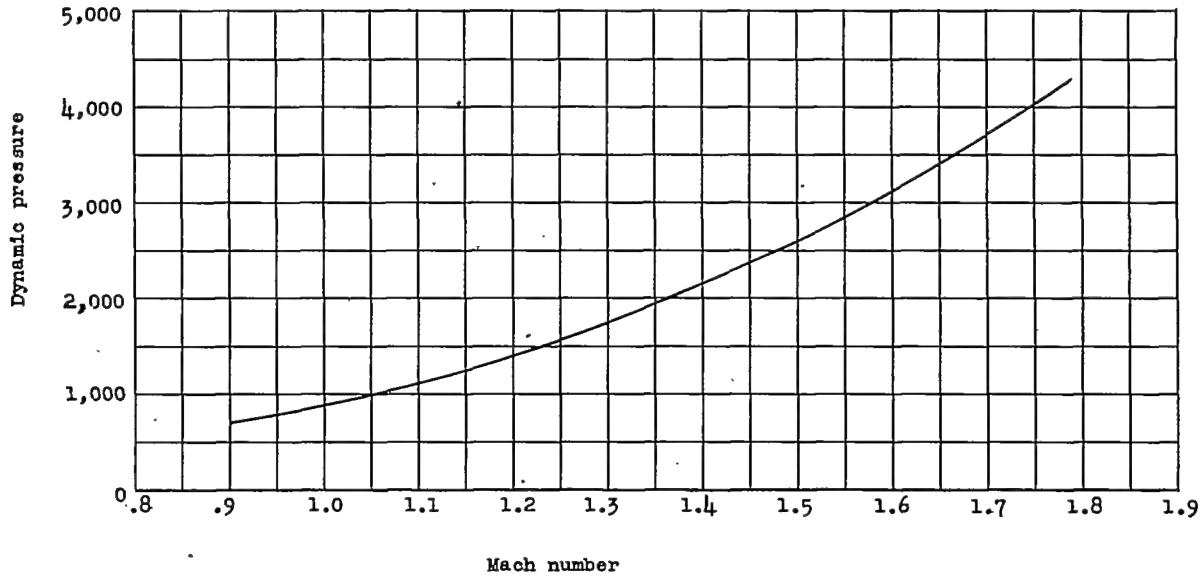

Figure 3.- Variation of dynamic pressure with Mach number.

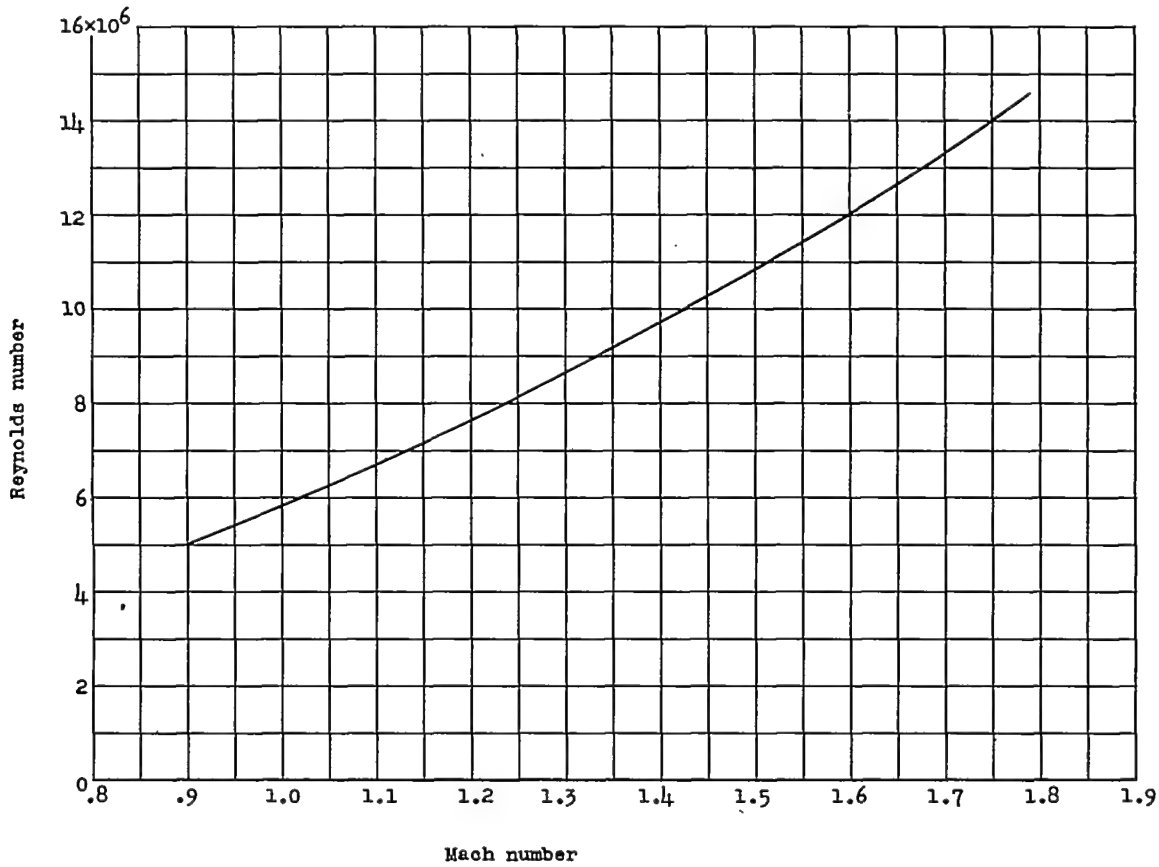

Figure 4.- Variation of Reynolds number with Mach number.

[redacted]

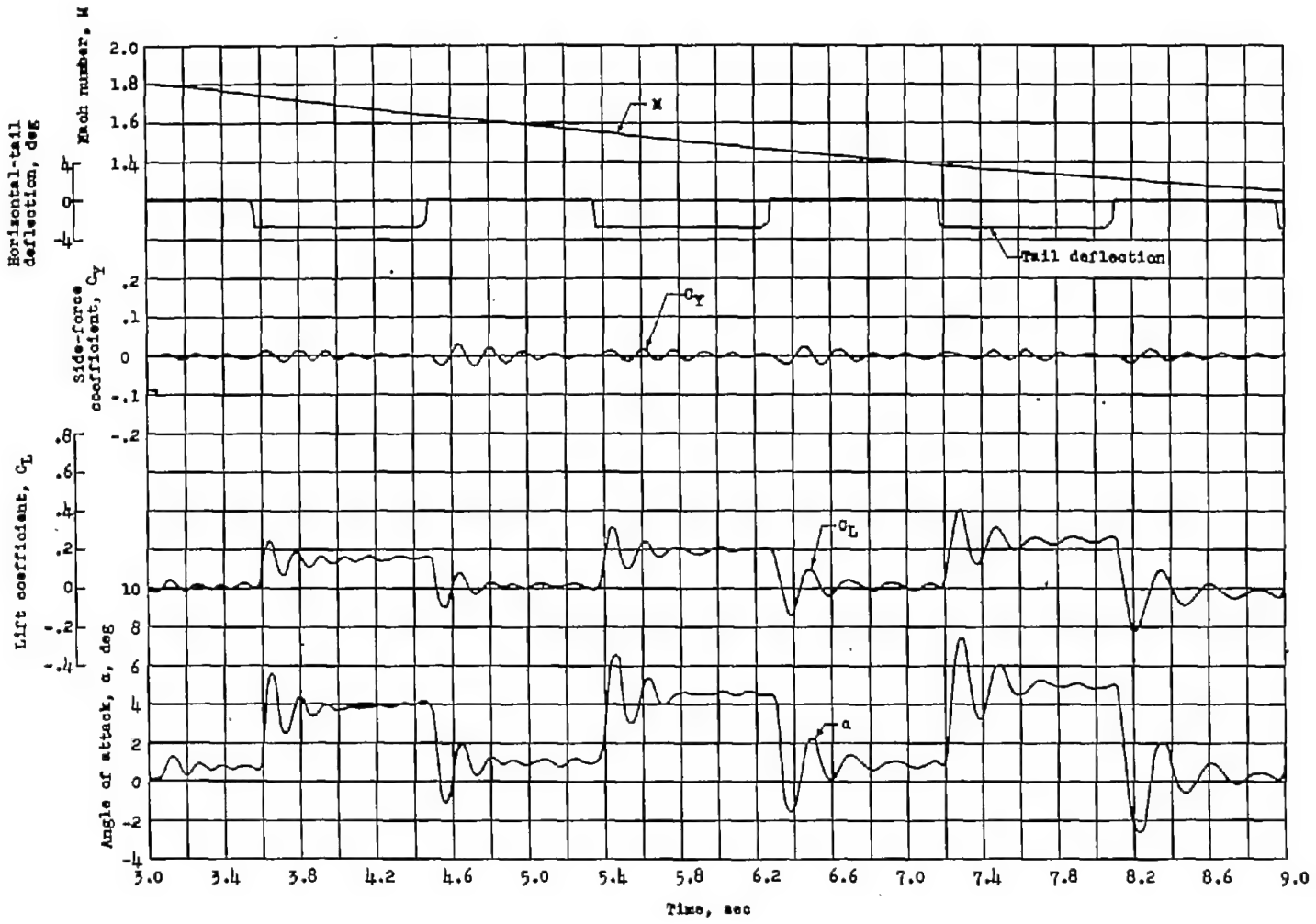

(a) Supersonic Mach numbers.

Figure 5.- Time history of some of the quantities measured in present investigation.

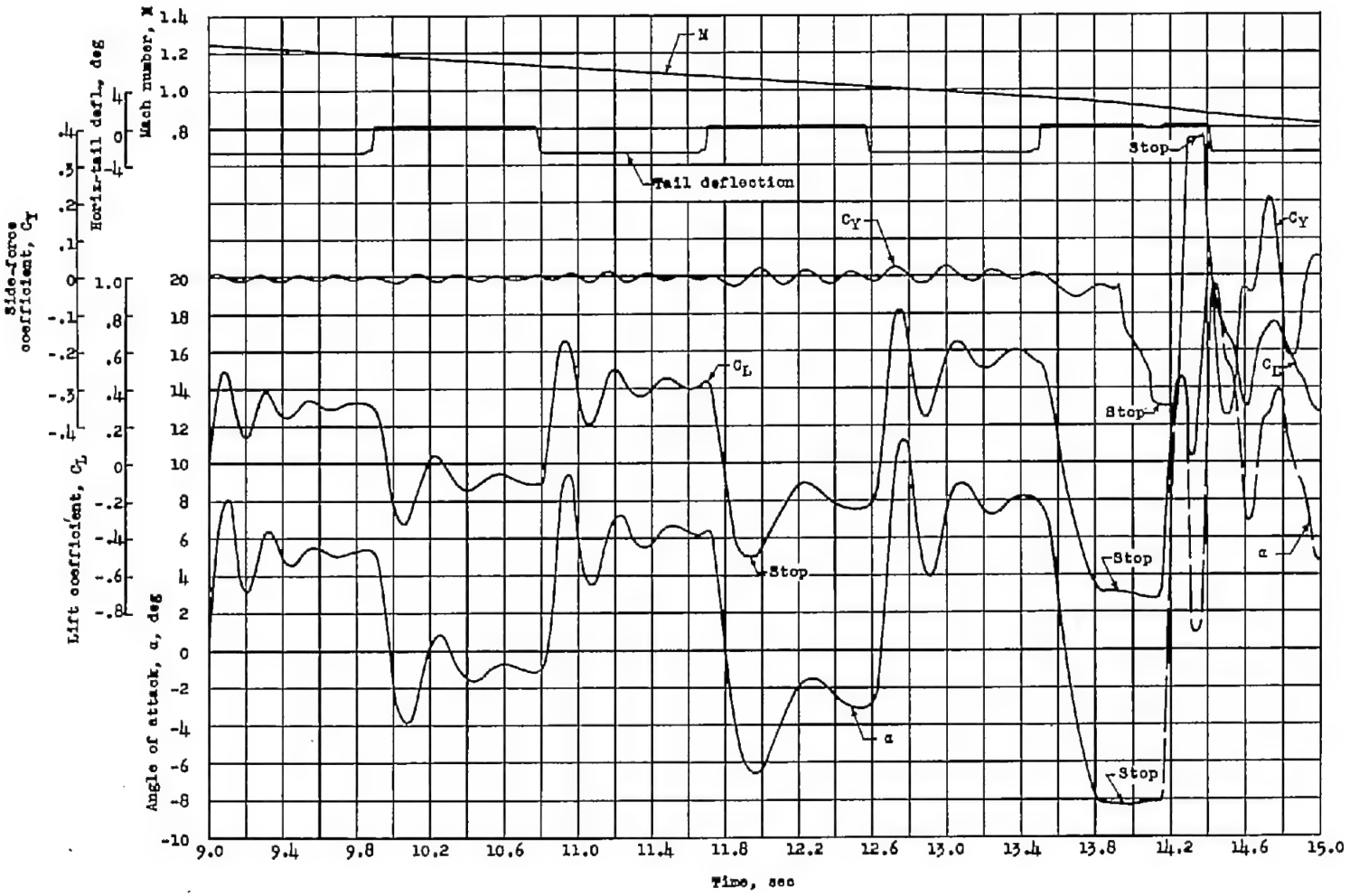

(b) Transonic Mach numbers.

Figure 5.- Concluded.

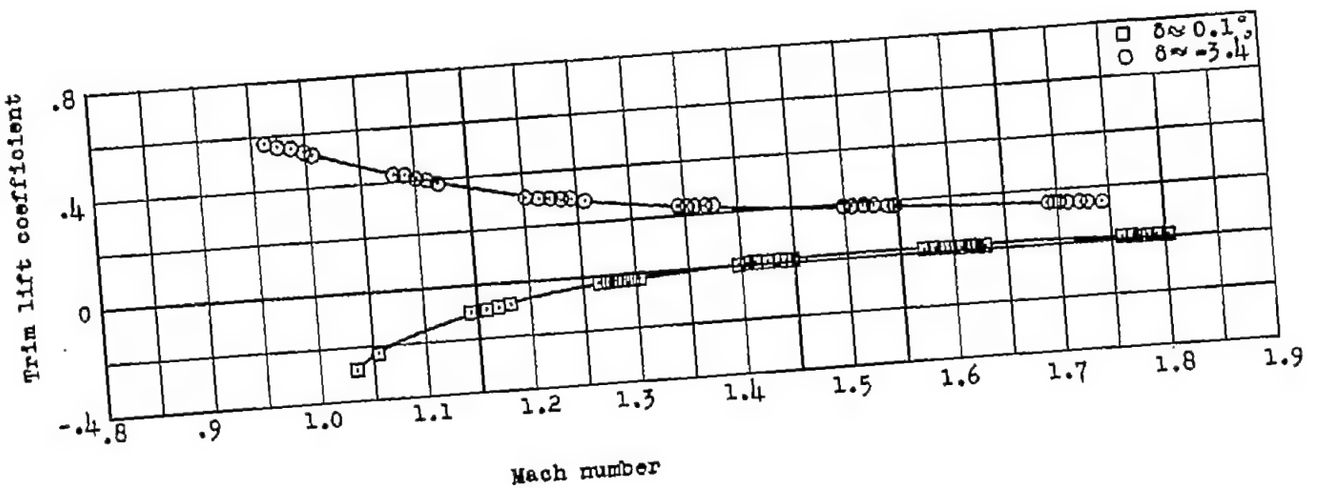

(a) Trim lift coefficient.

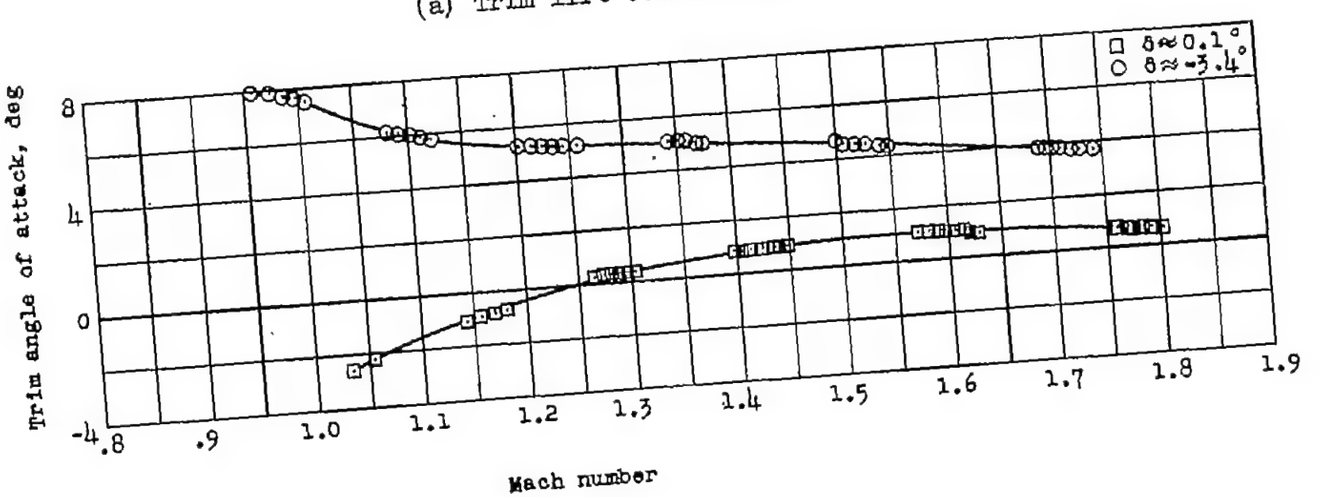

(b) Trim angle of attack.

Figure 6.- Longitudinal trim characteristics as a function of Mach number.

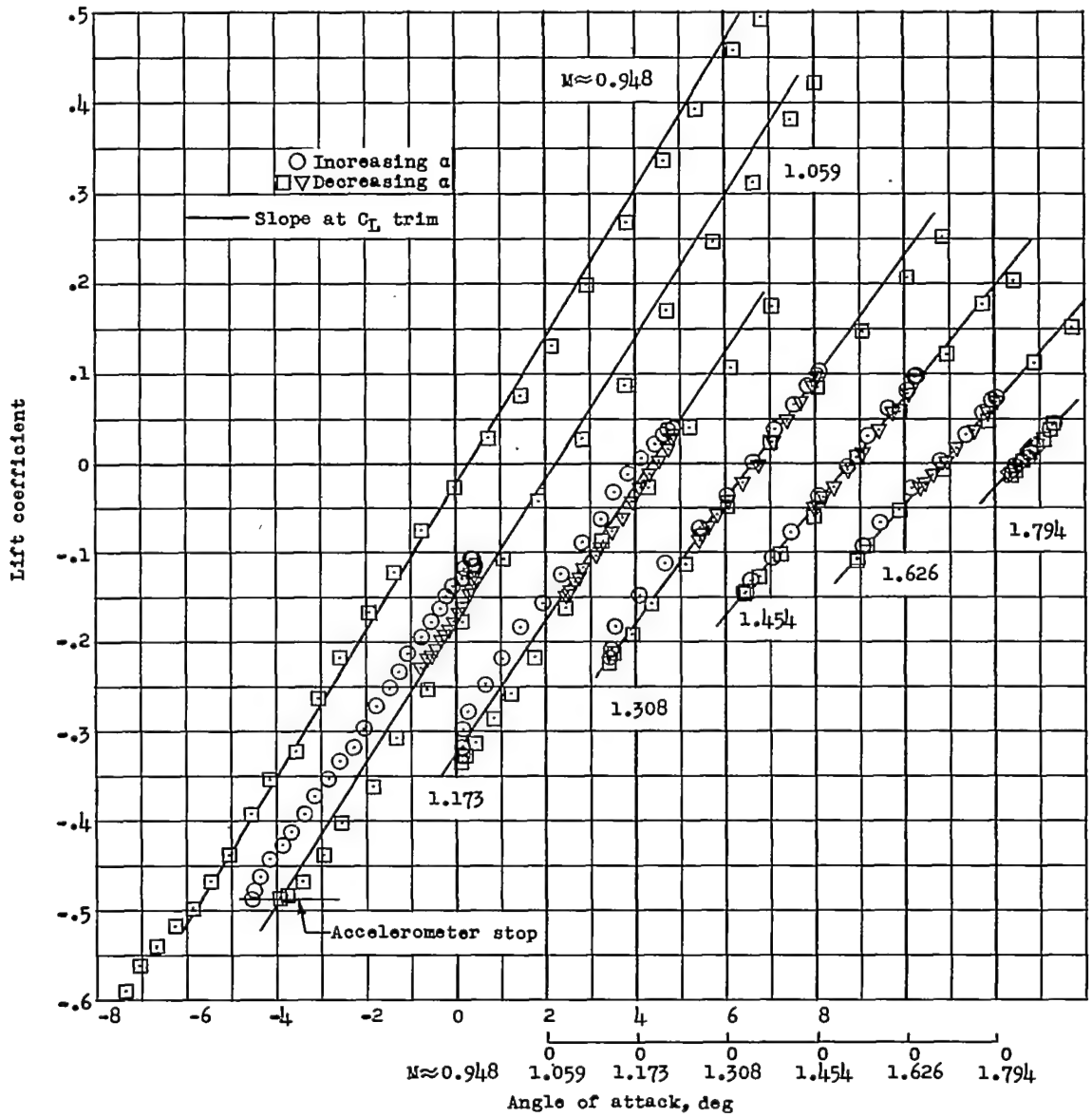

(a) $\delta \approx 0.1^{\circ}$.

Figure 7.- Variation of lift coefficient with angle of attack for the two tail settings.

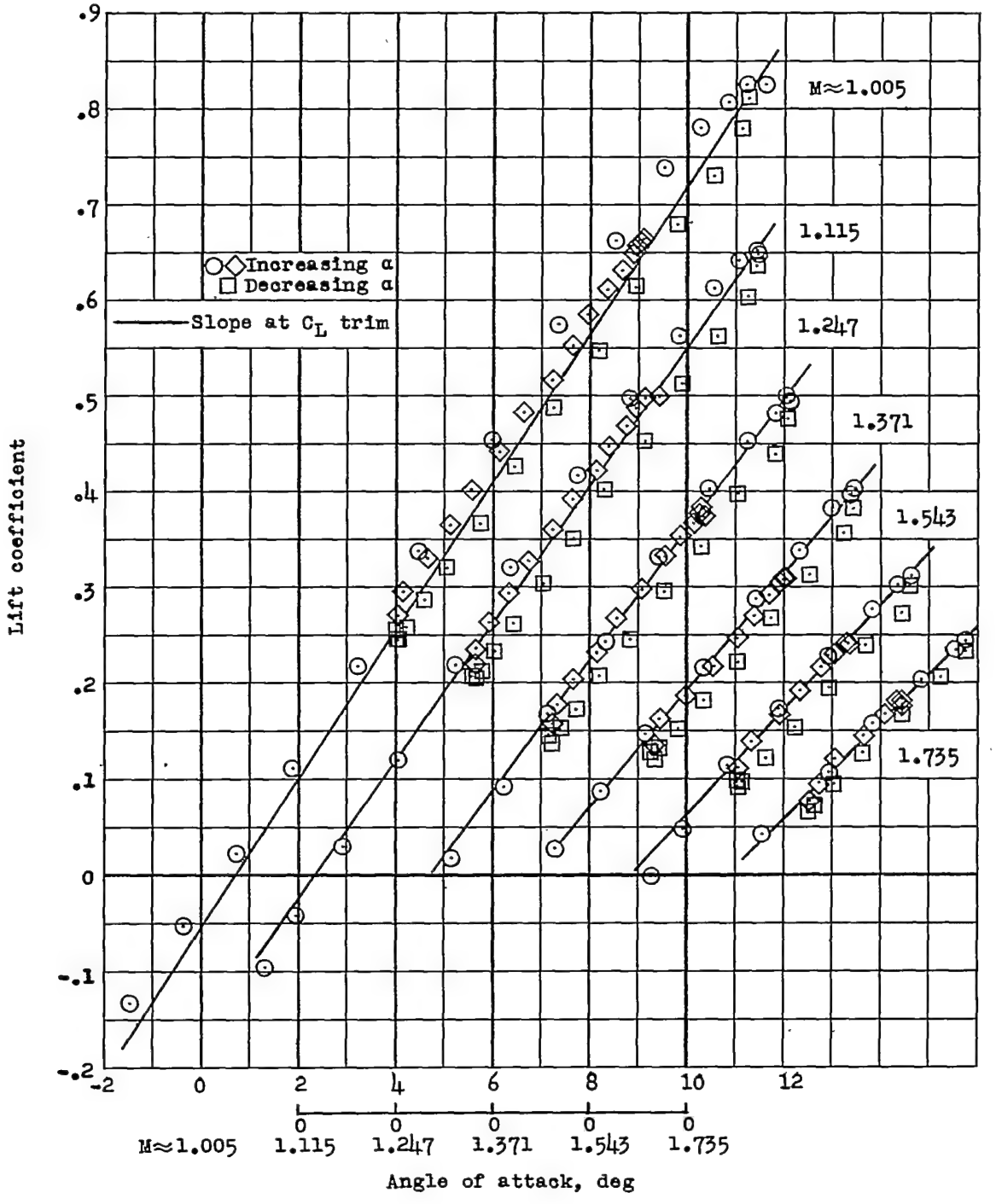

(b) $\delta \approx -3.4^{\circ}$.

Figure 7.- Concluded.

[redacted]

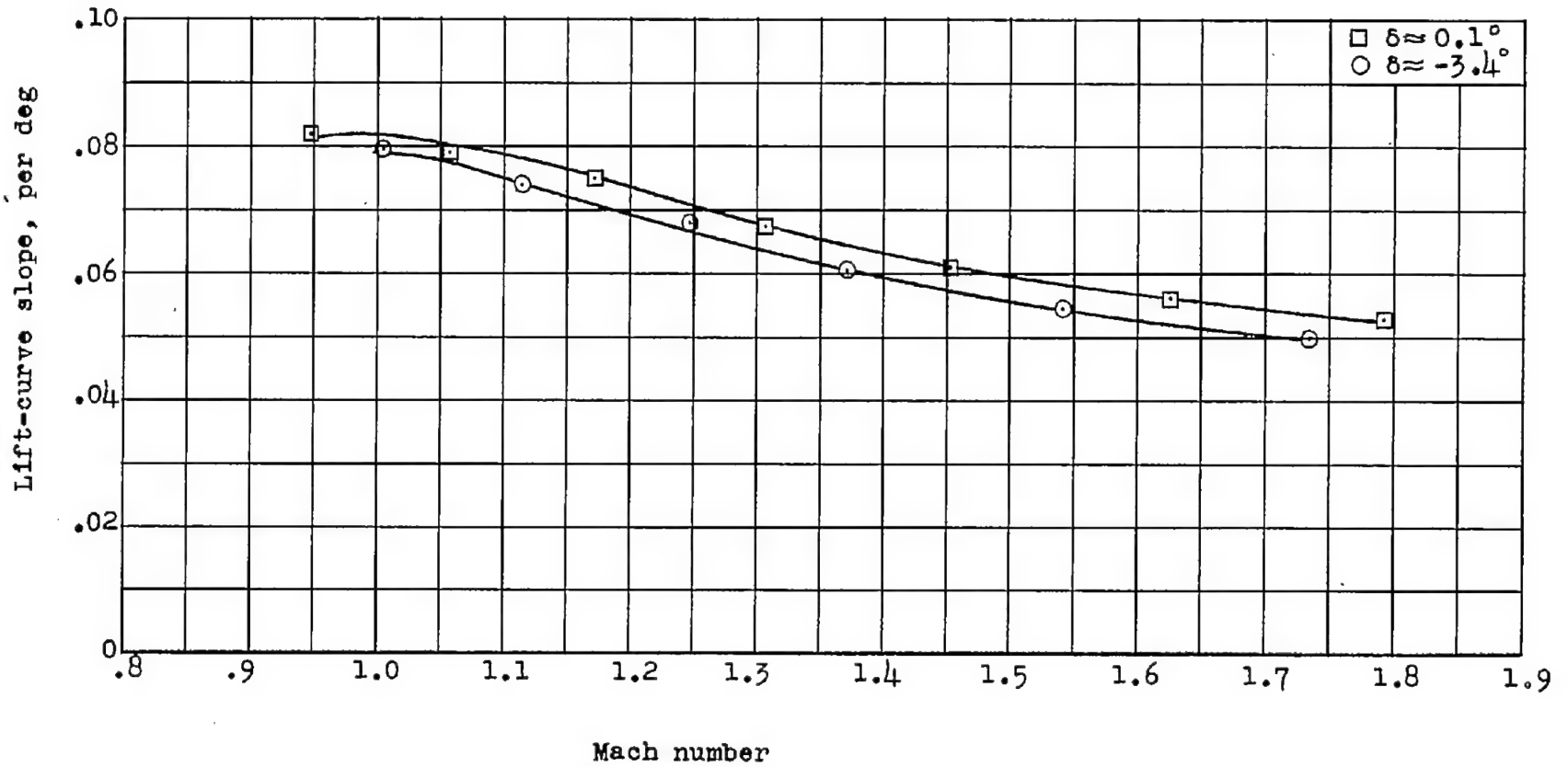

Figure 8.- Variation of lift-curve slope with Mach number.

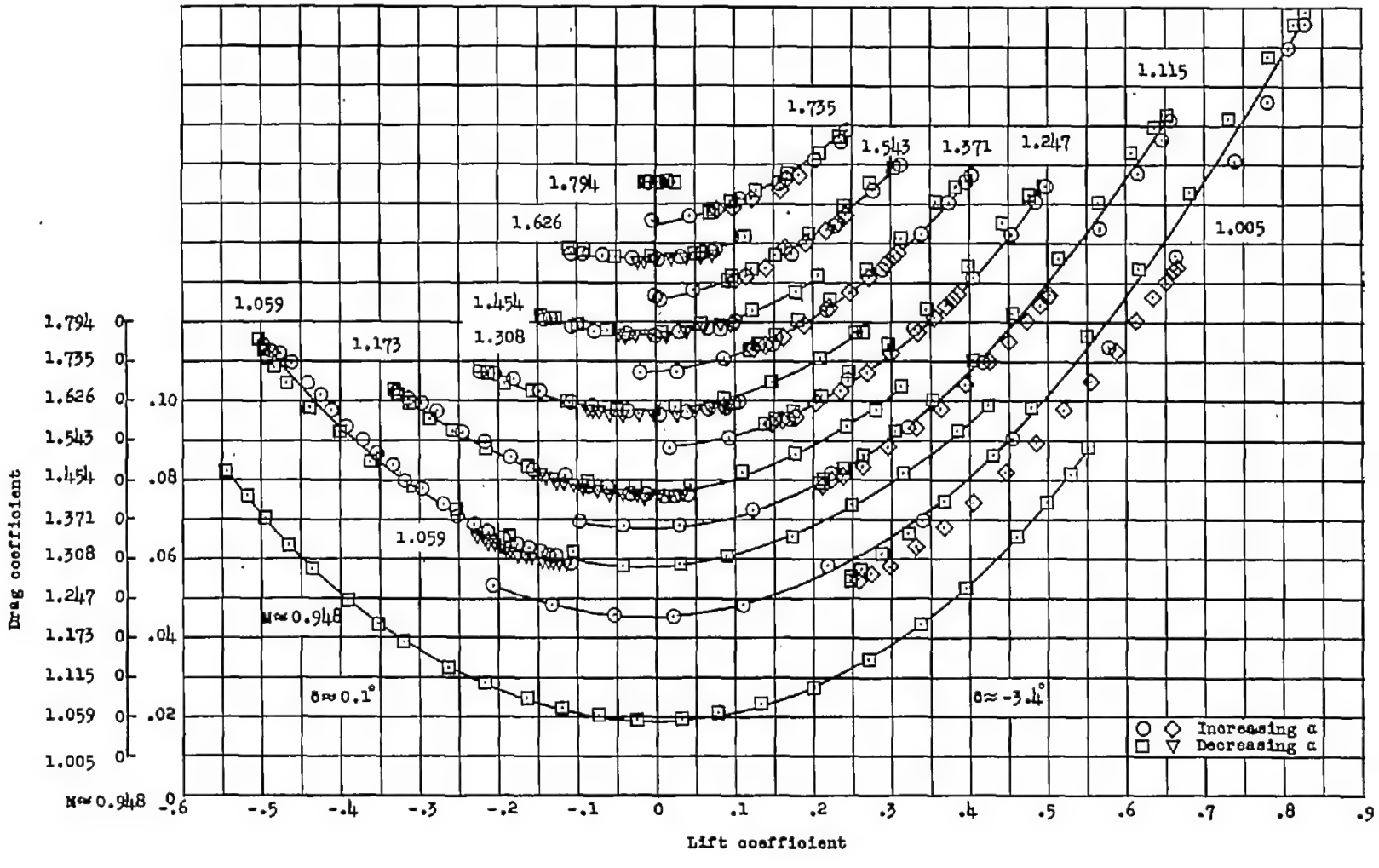

Figure 9.- Variation of drag with lift.

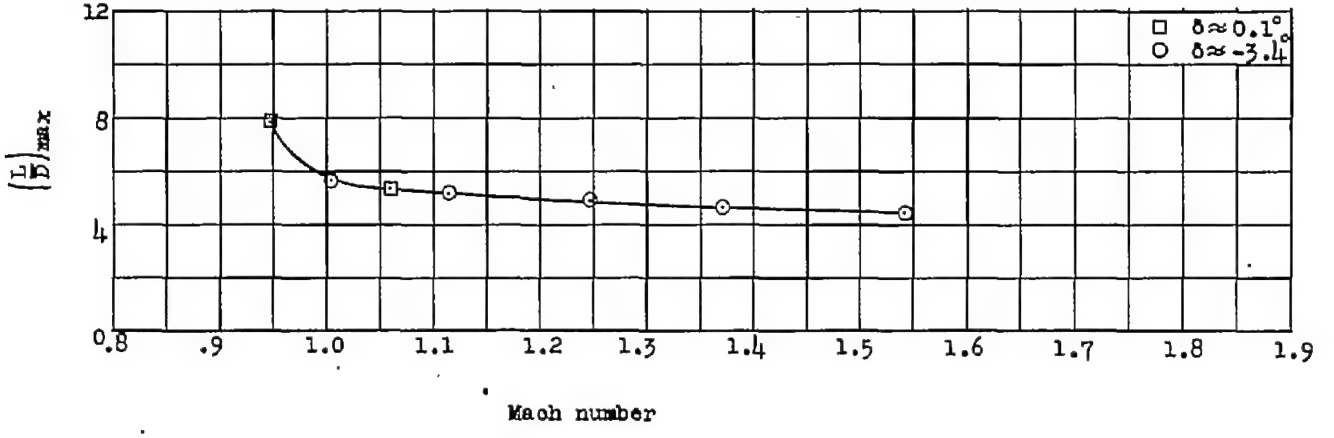

(a) Maximum lift-drag ratios.

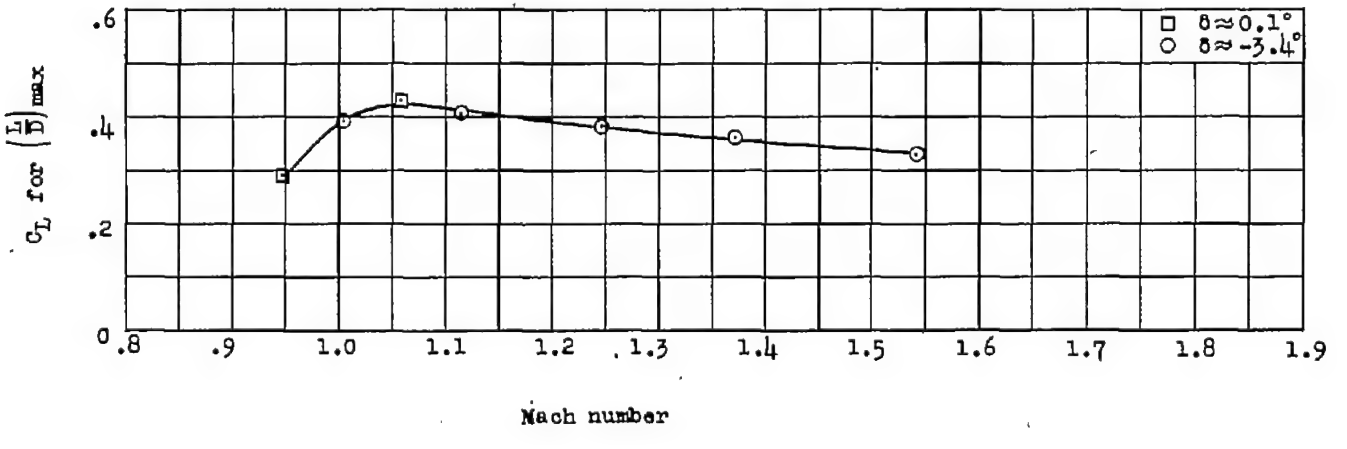

(b) Lift coefficients at which maximum lift-drag ratios occur.

Figure 10.- Variation of maximum lift-drag ratios and lift coefficients at which maximum lift-drag ratios occur as a function of Mach number.

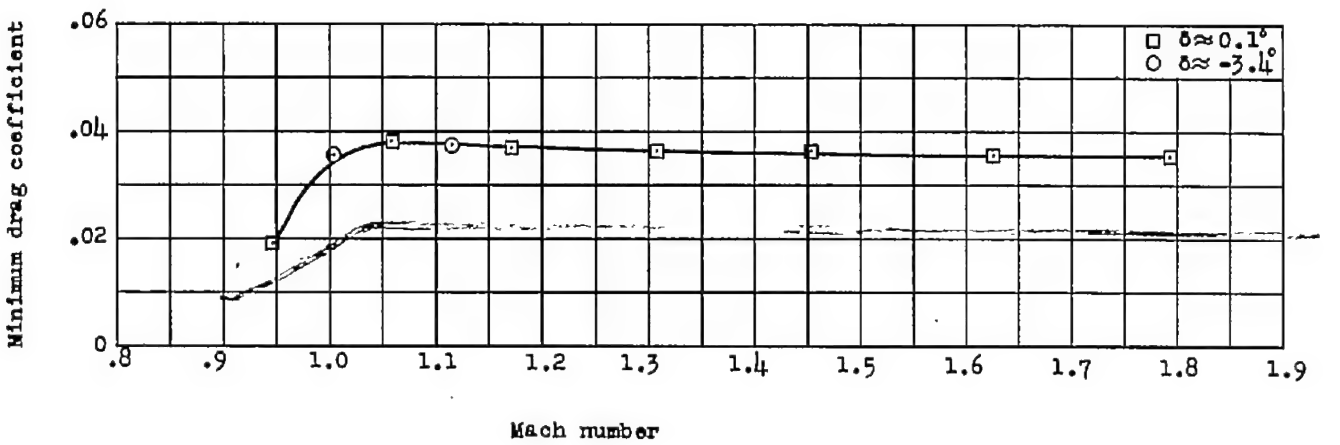

Figure 11.- Variation of minimum drag coefficient as a function of Mach number.

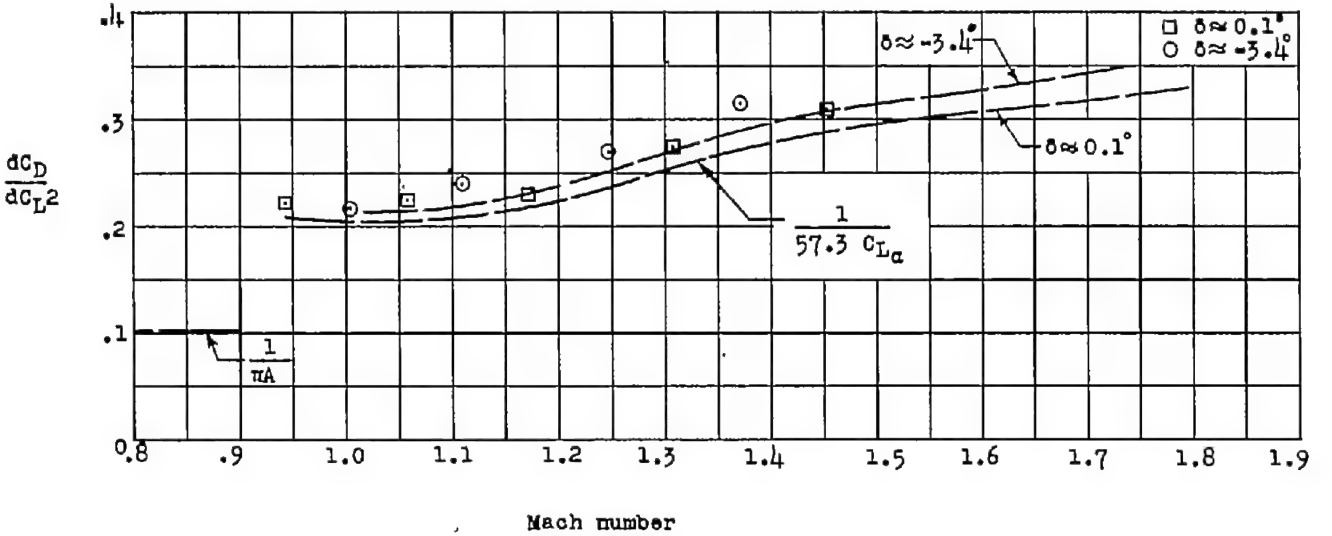

Figure 12.- Effect of lift on drag as a function of Mach number.

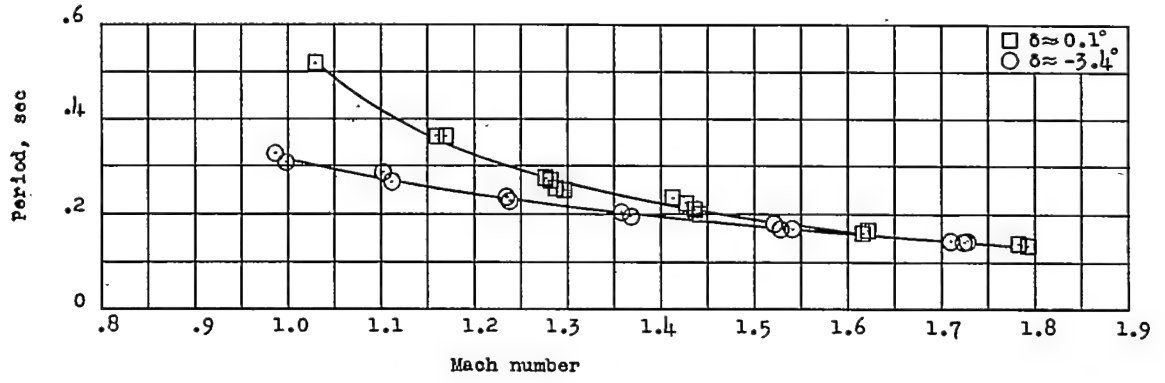

Figure 13.- Variation of measured period with Mach number.

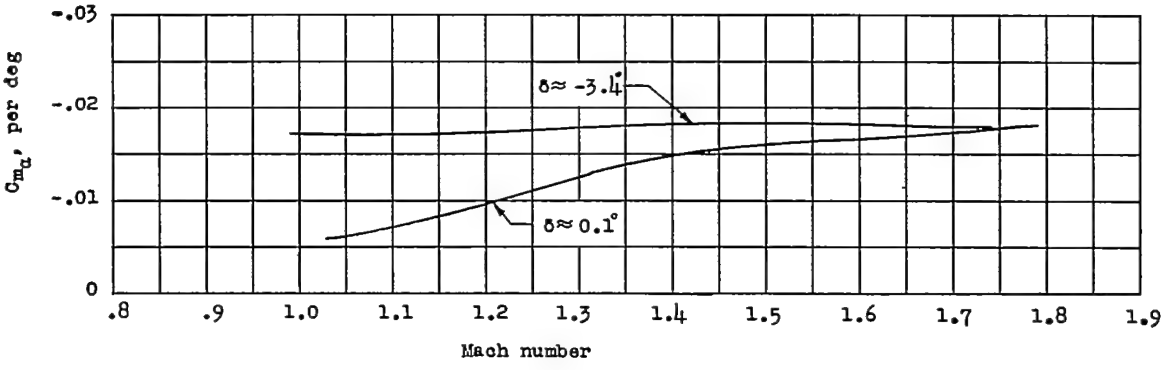

Figure 14.- Variation of static-stability parameter with Mach number.

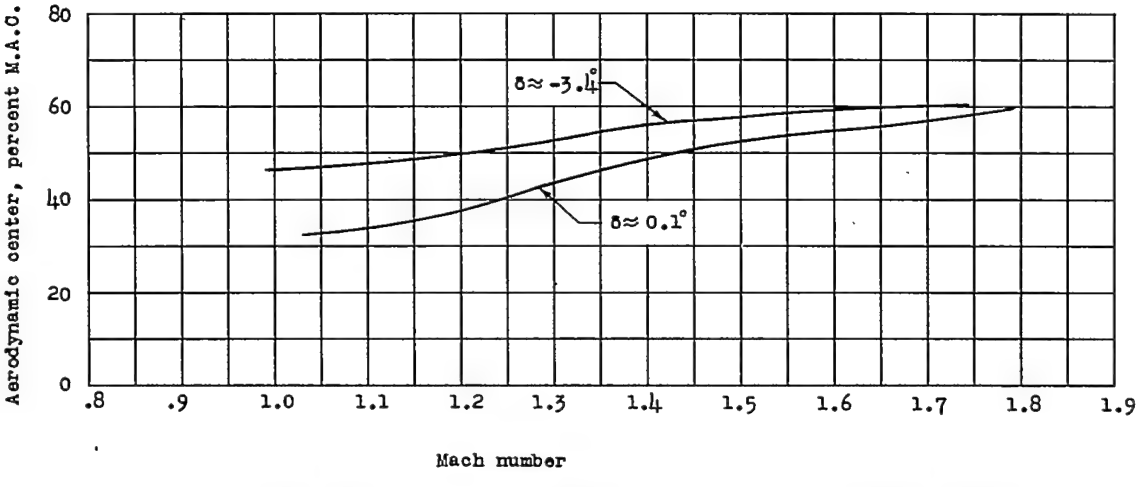

Figure 15.- Variation of aerodynamic center with Mach number.

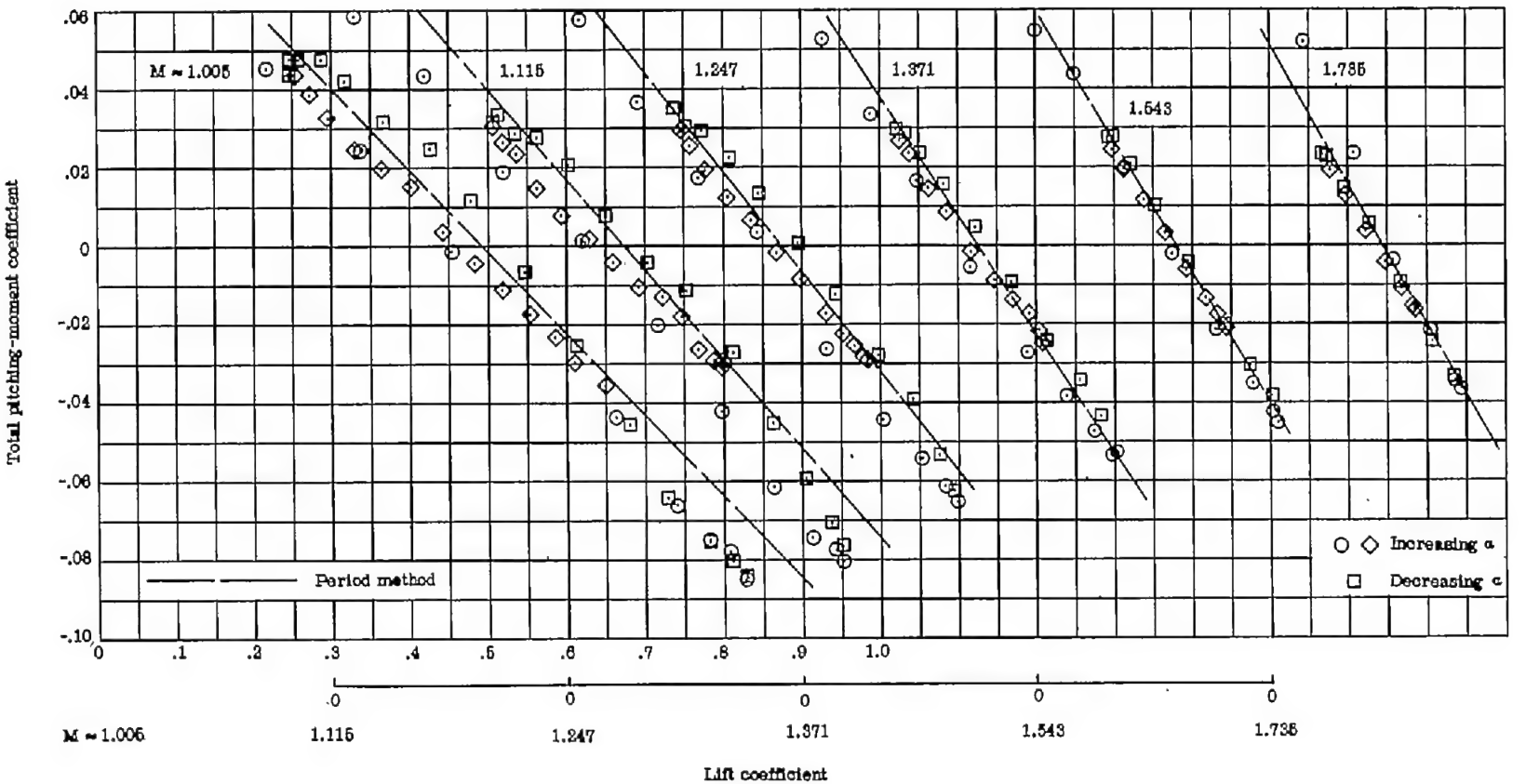

(a) $\delta \approx -3.4^{\circ}$.

Figure 16.- Variation of total pitching-moment coefficient with lift coefficient at the two tail settings.

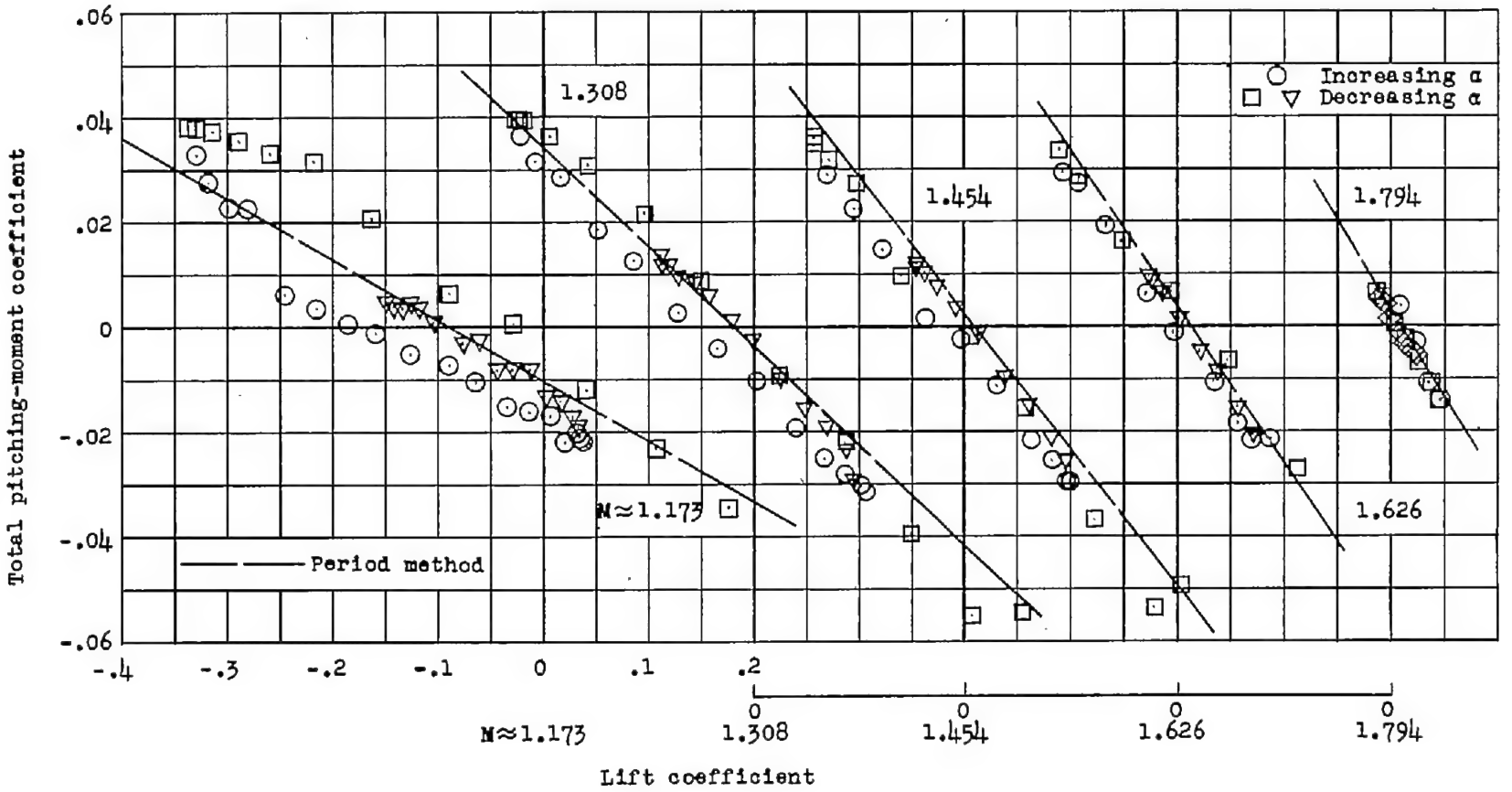

(b) $\delta \approx 0.1^{\circ}$.

Figure 16.- Continued.

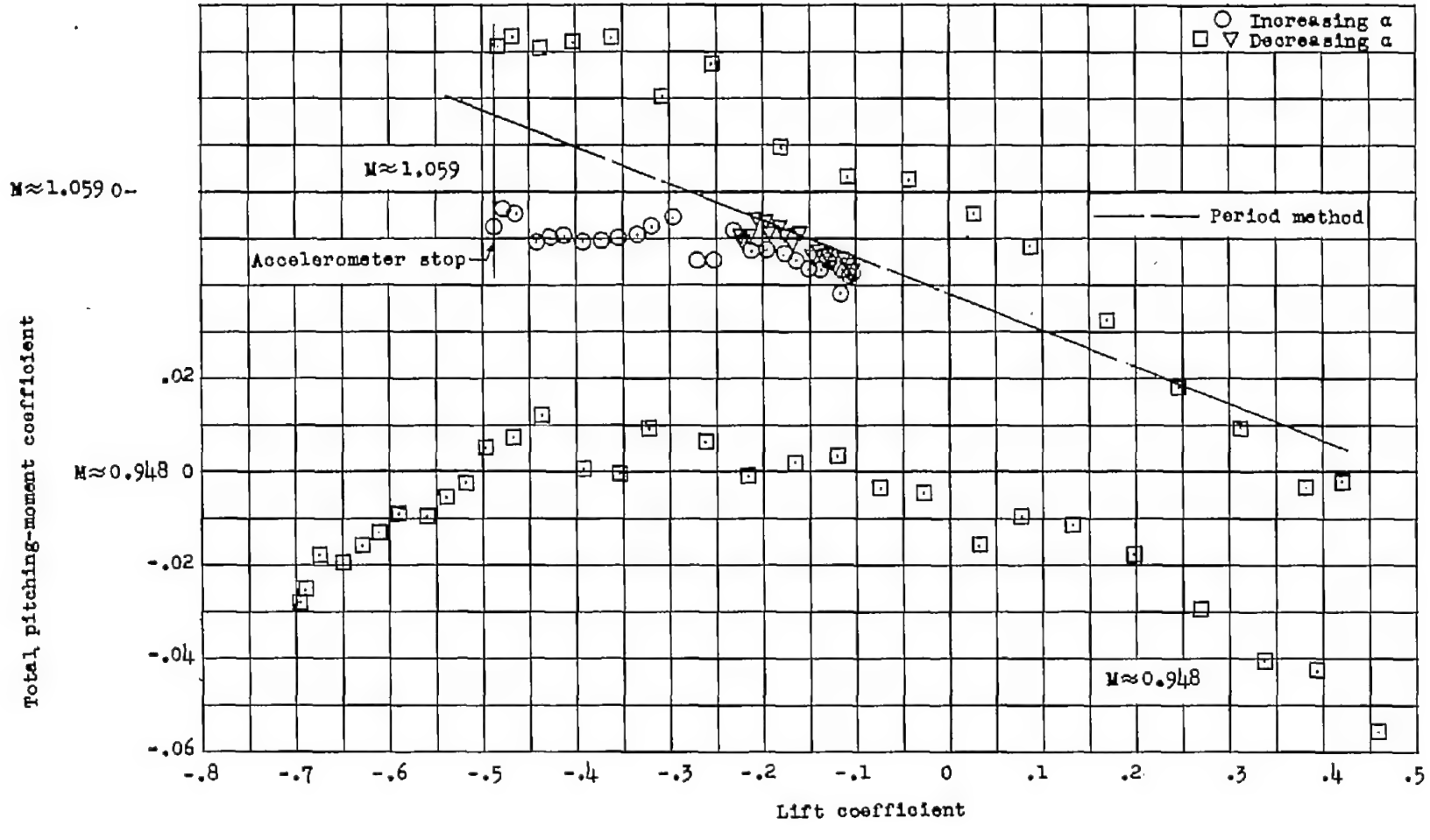

(b) $\delta \approx 0.1^{\circ}$.

Figure 16.- Concluded.

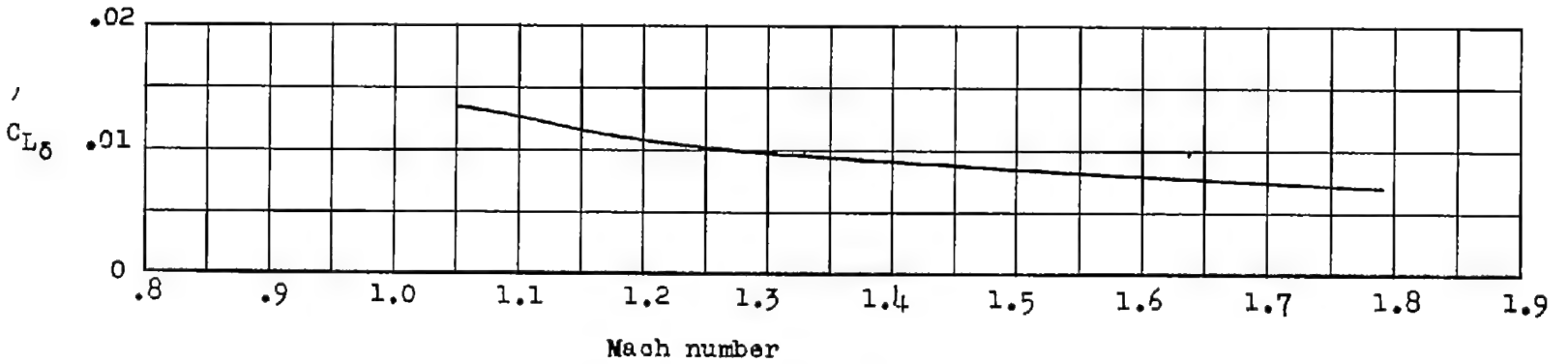

(a) Ability to produce lift.

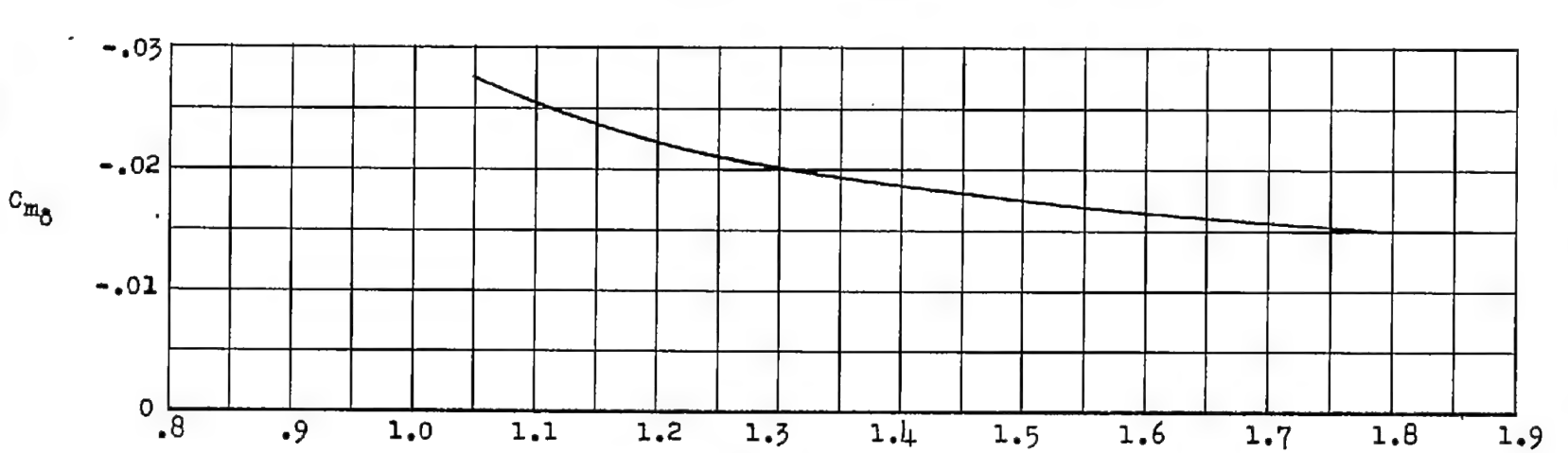

(b) Effectiveness in producing moment.

Figure 17.- Variation of ability of horizontal tail to produce lift and effectiveness in producing moment as a function of Mach number.

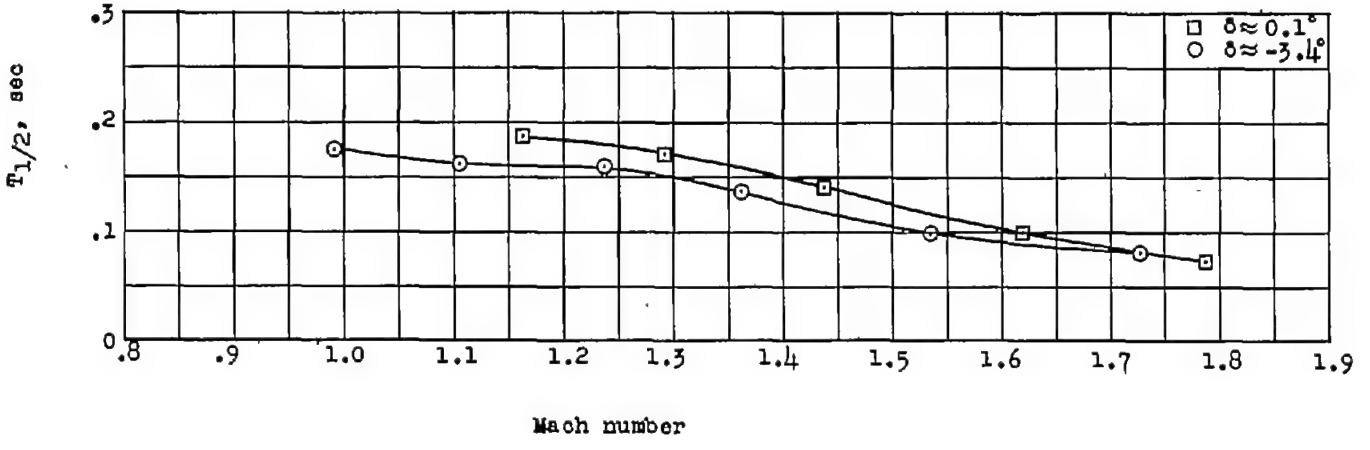

(a) Time to damp to one-half amplitude.

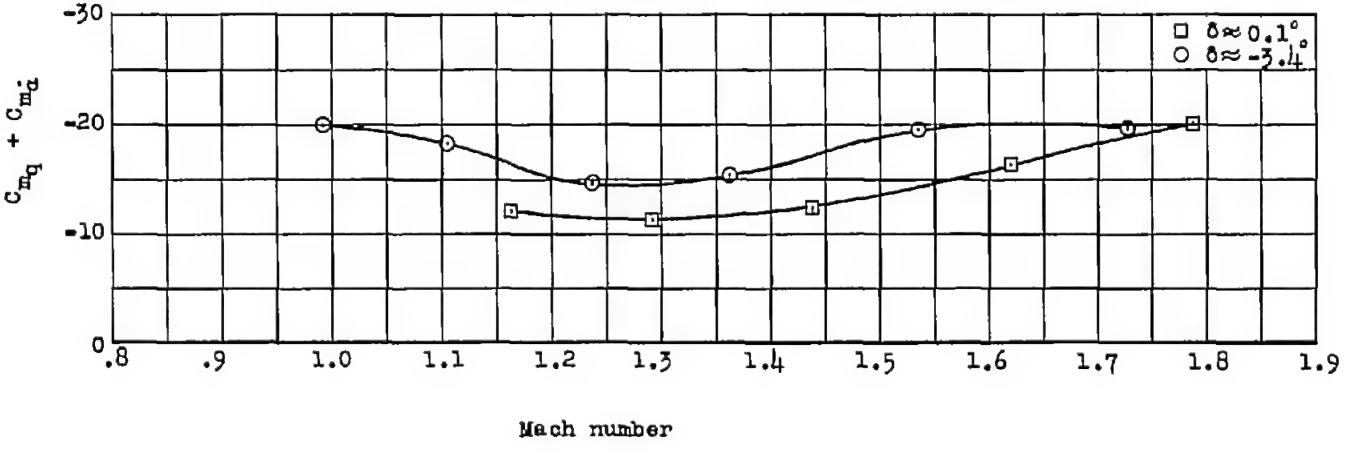

(b) Pitch damping-moment factor.

Figure 18.- Variation of damping characteristics of short-period oscillations with Mach number.

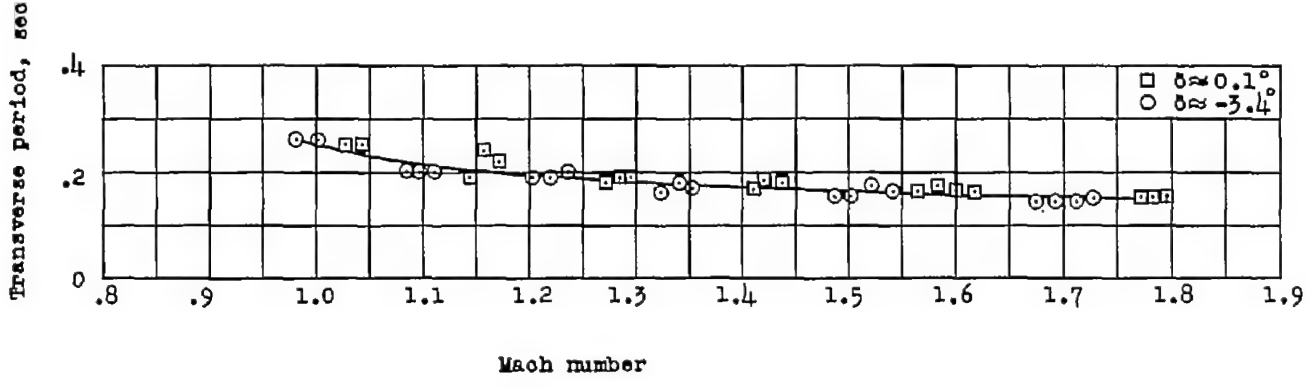

Figure 19.- Variation of measured period of lateral oscillation with Mach number.

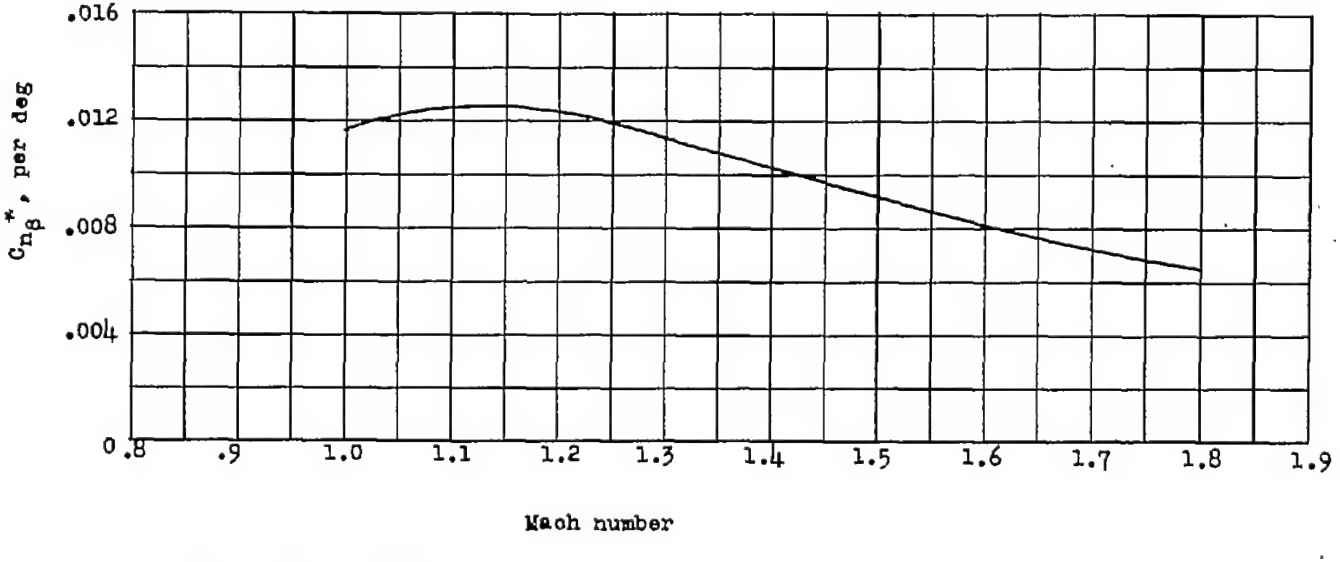

Figure 20.- Variation of static-directional-stability derivative with Mach number.

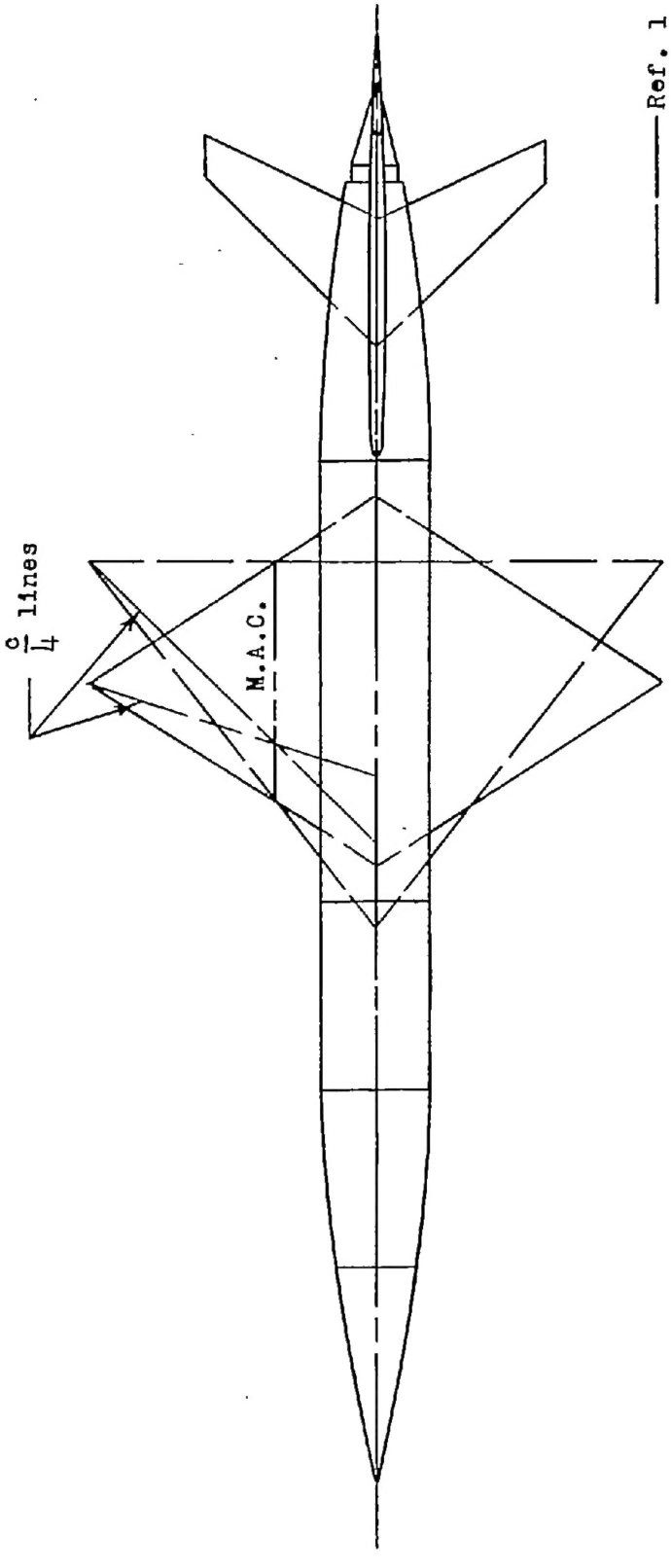

Figure 21.- Plan-form view of the two models superposed on each other.

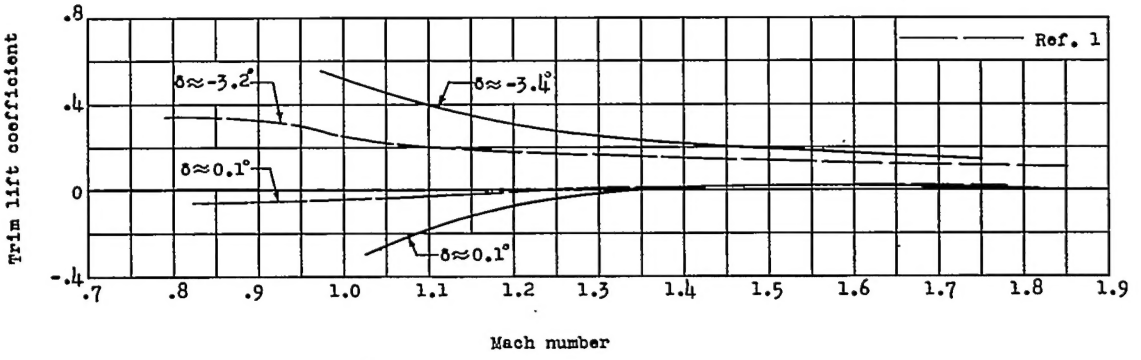

(a) Trim lift coefficients.

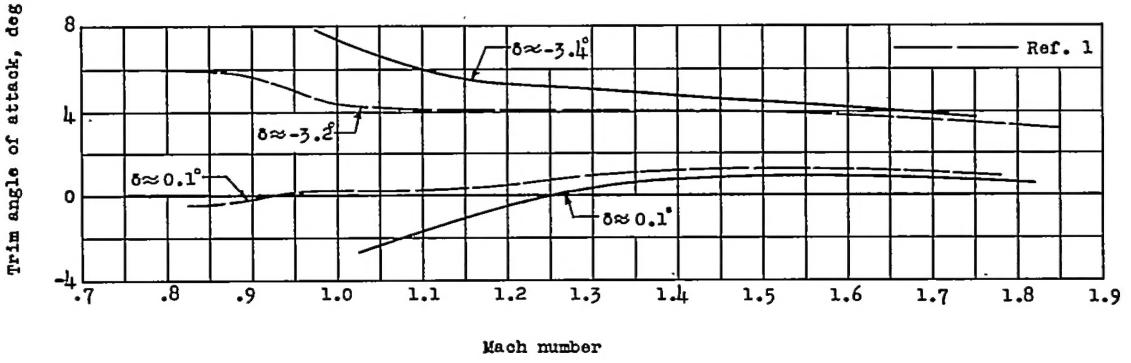

(b) Trim angles of attack.

Figure 22.- Longitudinal trim characteristics of the two models as a function of Mach number.

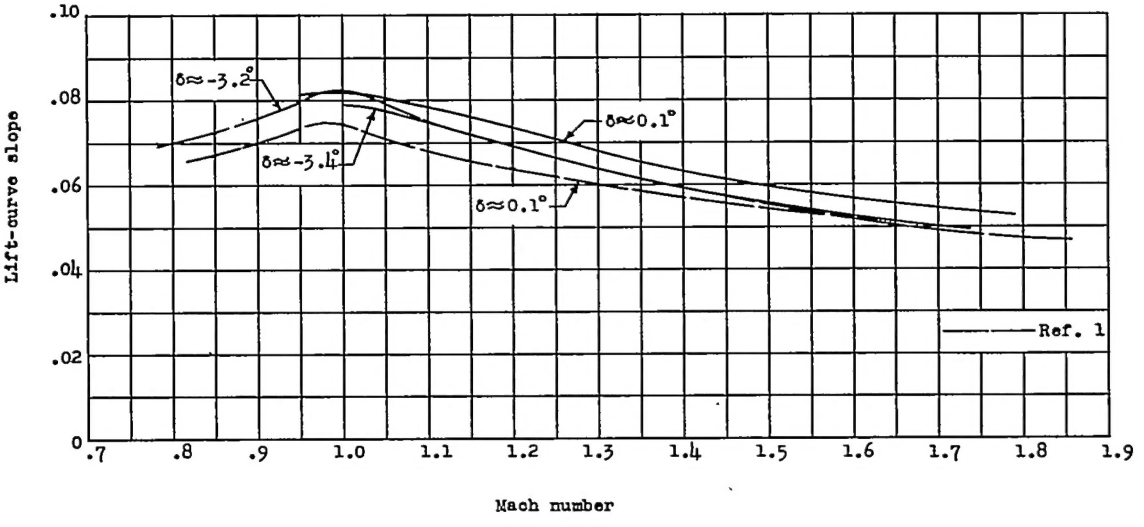

Figure 23.- Variation of lift-curve slopes with Mach number.

[redacted]

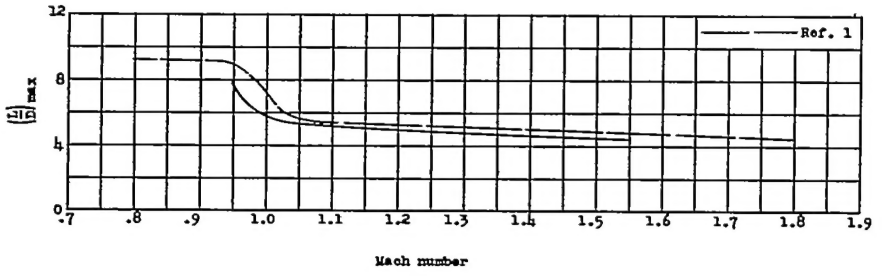

(a) Maximum lift-drag ratios.

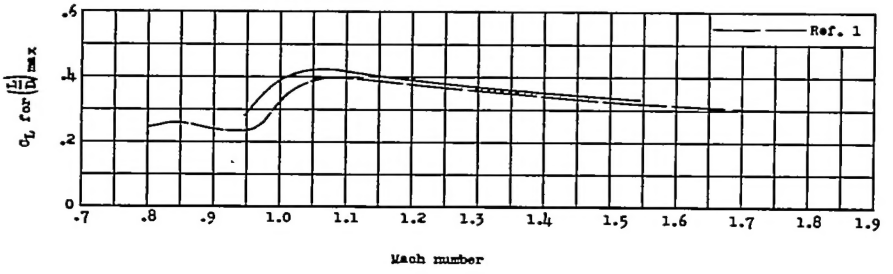

(b) Lift coefficients at which maximum lift-drag ratios occur.

Figure 24.- Variation of maximum lift-drag ratios and lift coefficients at which maximum lift-drag ratios occur as a function of Mach number.

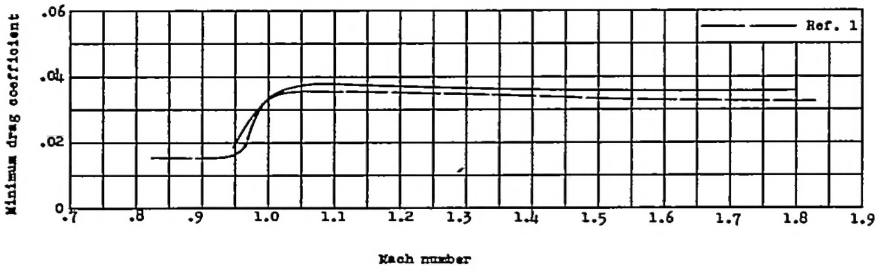

Figure 25.- Variation of minimum drag coefficient as a function of Mach number.

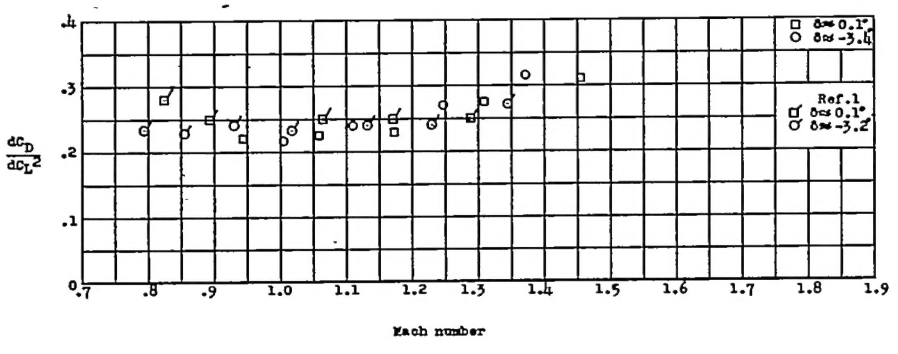

Figure 26.- Effect of lift on drag as a function of Mach number.

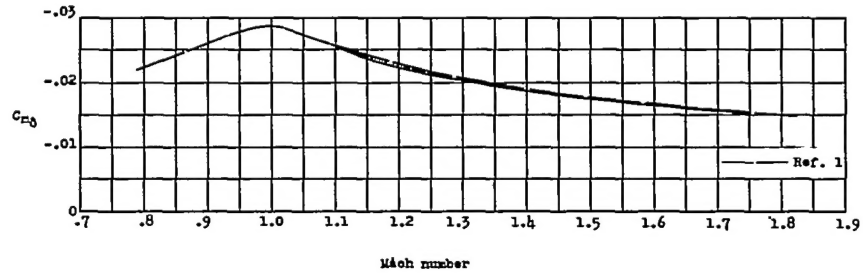

Figure 27.- Variation of the horizontal-tail effectiveness in producing moment as a function of Mach number.

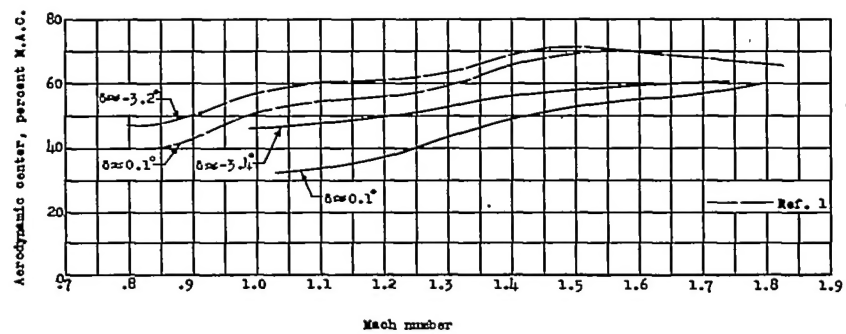

Figure 28.- Variation of aerodynamic center with Mach number.

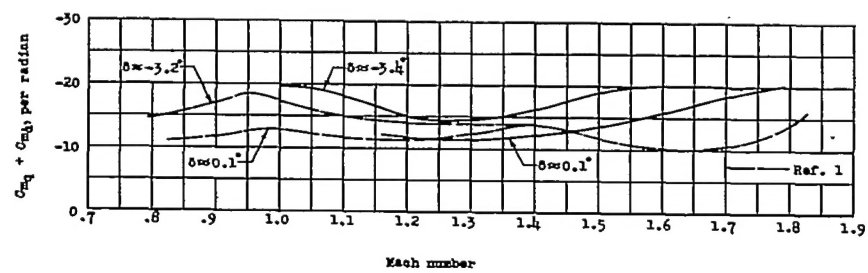

Figure 29.- Variation of the pitch damping-moment factors with Mach number.

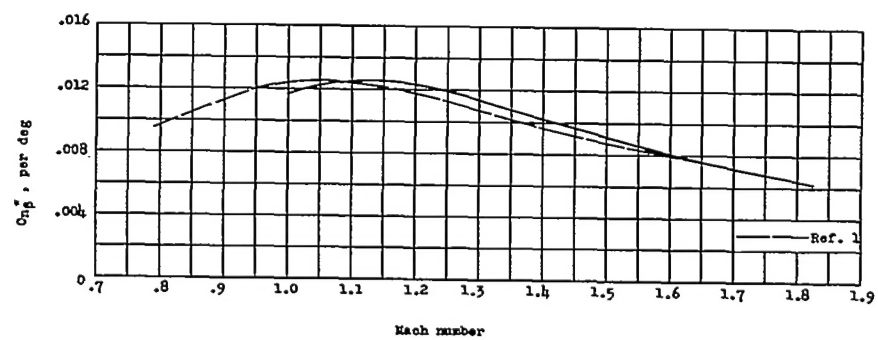

Figure 30.- Variation of static-directional-stability derivatives with Mach number.